MONKES: a fast neoclassical code for the evaluation of monoenergetic transport coefficients in stellarator plasmas

F. J. Escoto[1],

J. L. Velasco[1], I. Calvo[1], M. Landreman[2], F. I. Parra[3] and E. Sánchez[1]

[1]Laboratorio Nacional de Fusión, CIEMAT
[2]University of Maryland
[3]Princeton Plasma Physics Laboratory

August 14th, 2024

https://iopscience.iop.org/article/10.1088/1741-4326/ad3fc9
https://github.com/JavierEscoto/MONKES

MONKES paper

MONKES GitHub

Outline

1. Introduction
2. Drift-kinetic equation and transport coefficients
3. Algorithm
4. Benchmark and code performance
5. Some applications of `MONKES`
6. Conclusions and future work

Outline

1. Introduction
2. Drift-kinetic equation and transport coefficients
3. Algorithm
4. Benchmark and code performance
5. Some applications of `MONKES`
6. Conclusions and future work

Neoclassical transport and stellarator optimization

- Any stellarator candidate to fusion reactor must be close to omnigenity. W7-X has proven that optimization is effective [Beidler, Nature (2021)], [Dinklage, Nature Phys. (2018)].

Neoclassical transport and stellarator optimization

- Any stellarator candidate to fusion reactor must be close to omnigenity. W7-X has proven that optimization is effective [Beidler, Nature (2021)], [Dinklage, Nature Phys. (2018)].

- In order to optimize stellarators, we need to be able to evaluate neoclassical properties **fast**.

Neoclassical transport and stellarator optimization

- Any stellarator candidate to fusion reactor must be close to omnigenity. W7-X has proven that optimization is effective [Beidler, Nature (2021)], [Dinklage, Nature Phys. (2018)].

- In order to optimize stellarators, we need to be able to evaluate neoclassical properties **fast**.

- The optimization of neoclassical properties has been typically addressed **indirectly** (e.g. shaping $B-$contours) or using figures of merit:

Neoclassical transport and stellarator optimization

- Any stellarator candidate to fusion reactor must be close to omnigenity. W7-X has proven that optimization is effective [Beidler, Nature (2021)], [Dinklage, Nature Phys. (2018)].

- In order to optimize stellarators, we need to be able to evaluate neoclassical properties **fast**.

- The optimization of neoclassical properties has been typically addressed **indirectly** (e.g. shaping $B-$contours) or using figures of merit:
  - ✓ Radial transport in the $1/\nu$ is encapsulated in ϵ_{eff} [Nemov, PoP (1999)].

Neoclassical transport and stellarator optimization

- Any stellarator candidate to fusion reactor must be close to omnigenity. W7-X has proven that optimization is effective [Beidler, Nature (2021)], [Dinklage, Nature Phys. (2018)].

- In order to optimize stellarators, we need to be able to evaluate neoclassical properties **fast**.

- The optimization of neoclassical properties has been typically addressed **indirectly** (e.g. shaping $B-$contours) or using figures of merit:
  - ✓ Radial transport in the $1/\nu$ is encapsulated in ϵ_{eff} [Nemov, PoP (1999)].
  - ✗ Analytical formulas for the parallel flow in general magnetic geometry are not accurate.

Neoclassical transport and stellarator optimization

- Any stellarator candidate to fusion reactor must be close to omnigenity. W7-X has proven that optimization is effective [Beidler, Nature (2021)], [Dinklage, Nature Phys. (2018)].

- In order to optimize stellarators, we need to be able to evaluate neoclassical properties **fast**.

- The optimization of neoclassical properties has been typically addressed **indirectly** (e.g. shaping $B-$contours) or using figures of merit:
  - ✓ Radial transport in the $1/\nu$ is encapsulated in ϵ_{eff} [Nemov, PoP (1999)].
  - ✗ Analytical formulas for the parallel flow in general magnetic geometry are not accurate.

- Recent developments like the code `KNOSOS` [Velasco, JCP (2020)] permit **direct** optimization of radial neoclassical transport. However, it cannot give bootstrap current.

Neoclassical transport and stellarator optimization

- Any stellarator candidate to fusion reactor must be close to omnigenity. W7-X has proven that optimization is effective [Beidler, Nature (2021)], [Dinklage, Nature Phys. (2018)].

- In order to optimize stellarators, we need to be able to evaluate neoclassical properties **fast**.

- The optimization of neoclassical properties has been typically addressed **indirectly** (e.g. shaping $B-$contours) or using figures of merit:
  - ✓ Radial transport in the $1/\nu$ is encapsulated in ϵ_{eff} [Nemov, PoP (1999)].
  - ✗ Analytical formulas for the parallel flow in general magnetic geometry are not accurate.

- Recent developments like the code `KNOSOS` [Velasco, JCP (2020)] permit **direct** optimization of radial neoclassical transport. However, it cannot give bootstrap current.

- The next generation of stellarators should be optimized taking into account parallel transport.

Neoclassical transport and stellarator optimization

- Any stellarator candidate to fusion reactor must be close to omnigenity. W7-X has proven that optimization is effective [Beidler, Nature (2021)], [Dinklage, Nature Phys. (2018)].

- In order to optimize stellarators, we need to be able to evaluate neoclassical properties **fast**.

- The optimization of neoclassical properties has been typically addressed **indirectly** (e.g. shaping $B-$contours) or using figures of merit:
  - ✓ Radial transport in the $1/\nu$ is encapsulated in ϵ_{eff} [Nemov, PoP (1999)].
  - ✗ Analytical formulas for the parallel flow in general magnetic geometry are not accurate.

- Recent developments like the code `KNOSOS` [Velasco, JCP (2020)] permit **direct** optimization of radial neoclassical transport. However, it cannot give bootstrap current.

- The next generation of stellarators should be optimized taking into account parallel transport.
  - In quasi-symmetric (QS) stellarators, the bootstrap current can be large and its effect on the magnetic configuration must be included in the optimization process.

Neoclassical transport and stellarator optimization

- Any stellarator candidate to fusion reactor must be close to omnigenity. W7-X has proven that optimization is effective [Beidler, Nature (2021)], [Dinklage, Nature Phys. (2018)].

- In order to optimize stellarators, we need to be able to evaluate neoclassical properties **fast**.

- The optimization of neoclassical properties has been typically addressed **indirectly** (e.g. shaping $B-$contours) or using figures of merit:
  - ✓ Radial transport in the $1/\nu$ is encapsulated in ϵ_{eff} [Nemov, PoP (1999)].
  - ✗ Analytical formulas for the parallel flow in general magnetic geometry are not accurate.

- Recent developments like the code `KNOSOS` [Velasco, JCP (2020)] permit **direct** optimization of radial neoclassical transport. However, it cannot give bootstrap current.

- The next generation of stellarators should be optimized taking into account parallel transport.
  - In quasi-symmetric (QS) stellarators, the bootstrap current can be large and its effect on the magnetic configuration must be included in the optimization process.
  - In quasi-isodynamic (QI) fields (omnigenous + poloidally closed $B-$contours), one needs to check that the current is small (is zero for QI magnetic fields) or minimize it **directly**.

Neoclassical transport and stellarator optimization

- Any stellarator candidate to fusion reactor must be close to omnigenity. W7-X has proven that optimization is effective [Beidler, Nature (2021)], [Dinklage, Nature Phys. (2018)].

- In order to optimize stellarators, we need to be able to evaluate neoclassical properties **fast**.

- The optimization of neoclassical properties has been typically addressed **indirectly** (e.g. shaping $B-$contours) or using figures of merit:
  - ✓ Radial transport in the $1/\nu$ is encapsulated in ϵ_{eff} [Nemov, PoP (1999)].
  - ✗ Analytical formulas for the parallel flow in general magnetic geometry are not accurate.

- Recent developments like the code `KNOSOS` [Velasco, JCP (2020)] permit **direct** optimization of radial neoclassical transport. However, it cannot give bootstrap current.

- The next generation of stellarators should be optimized taking into account parallel transport.
  - In quasi-symmetric (QS) stellarators, the bootstrap current can be large and its effect on the magnetic configuration must be included in the optimization process.
  - In quasi-isodynamic (QI) fields (omnigenous + poloidally closed $B-$contours), one needs to check that the current is small (is zero for QI magnetic fields) or minimize it **directly**.

In the past, for general magnetic geometry, **an accurate calculation of the bootstrap current was too slow** to include it in the optimization process.

Neoclassical transport simulations for understanding experiments

- In order to understand plasma discharges in stellarators and improve our theoretical knowledge, profile prediction simulations are crucial.

Neoclassical transport simulations for understanding experiments

- In order to understand plasma discharges in stellarators and improve our theoretical knowledge, profile prediction simulations are crucial.
- Plasma density and temperature profiles can be predicted using neoclassical transport coefficients with the `NTSS` code [Turkin, PoP (2011)].

Neoclassical transport simulations for understanding experiments

- In order to understand plasma discharges in stellarators and improve our theoretical knowledge, profile prediction simulations are crucial.
- Plasma density and temperature profiles can be predicted using neoclassical transport coefficients with the `NTSS` code [Turkin, PoP (2011)].
- Recent developments like `Trinity-GX` [Mandell, APS (2023)] or `TANGO` [Bañón, NF (2023)] combine accurate calculations of turbulent and neoclassical transport for self-consistent profile evolution.

Neoclassical transport simulations for understanding experiments

- In order to understand plasma discharges in stellarators and improve our theoretical knowledge, profile prediction simulations are crucial.
- Plasma density and temperature profiles can be predicted using neoclassical transport coefficients with the **`NTSS`** code [Turkin, PoP (2011)].
- Recent developments like **`Trinity-GX`** [Mandell, APS (2023)] or **`TANGO`** [Bañón, NF (2023)] combine accurate calculations of turbulent and neoclassical transport for self-consistent profile evolution.
- In the past, an accurate calculation of the bootstrap current in general magnetic geometry was too slow to be included systematically in predictive transport frameworks.

Neoclassical transport simulations for understanding experiments

- In order to understand plasma discharges in stellarators and improve our theoretical knowledge, profile prediction simulations are crucial.
- Plasma density and temperature profiles can be predicted using neoclassical transport coefficients with the `NTSS` code [Turkin, PoP (2011)].
- Recent developments like `Trinity-GX` [Mandell, APS (2023)] or `TANGO` [Bañón, NF (2023)] combine accurate calculations of turbulent and neoclassical transport for self-consistent profile evolution.
- In the past, an accurate calculation of the bootstrap current in general magnetic geometry was too slow to be included systematically in predictive transport frameworks.

In this talk: the code `MONKES` (MONoenergetic Kinetic Equation Solver) will be presented, conceived to satisfy the necessity of **fast and accurate** calculations of the bootstrap current in stellarators.
Thus, it opens up the possibilities of **direct optimization of neoclassical transport** and to include the bootstrap curent effect in **predictive transport simulations**.

Outline

Drift-kinetic equation (DKE)

`MONKES` solves the same equation as `DKES` [Hirshman, Phys. Fluids (1986)] for the species a

$$(v\xi\boldsymbol{b} + \boldsymbol{v}_E)\cdot\nabla h_a + v\nabla\cdot\boldsymbol{b}\frac{(1-\xi^2)}{2}\frac{\partial h_a}{\partial\xi} - \nu^a\mathcal{L}h_a = S_a,$$

where h_a is the deviation of the distribution function from a Maxwellian, $v := |\boldsymbol{v}|$, $\xi := \boldsymbol{v}\cdot\boldsymbol{b}/v$, $\boldsymbol{v}_E := -E_\psi(\psi)\boldsymbol{B}\times\nabla\psi/\left\langle B^2\right\rangle$, ψ is the flux-surface label and $\mathcal{L} := \frac{1}{2}\,\partial/\partial\xi\,\left((1-\xi^2)\,\partial/\partial\xi\right)$.

Drift-kinetic equation (DKE)

`MONKES` solves the same equation as `DKES` [Hirshman, Phys. Fluids (1986)] for the species a

$$(v\xi\boldsymbol{b} + \boldsymbol{v}_E)\cdot\nabla h_a + v\nabla\cdot\boldsymbol{b}\frac{(1-\xi^2)}{2}\frac{\partial h_a}{\partial \xi} - \nu^a \mathcal{L} h_a = S_a,$$

where h_a is the deviation of the distribution function from a Maxwellian, $v := |\boldsymbol{v}|$, $\xi := \boldsymbol{v}\cdot\boldsymbol{b}/v$, $\boldsymbol{v}_E := -E_\psi(\psi)\boldsymbol{B}\times\nabla\psi/\langle B^2\rangle$, ψ is the flux-surface label and $\mathcal{L} := \frac{1}{2}\,\partial/\partial\xi\,\left((1-\xi^2)\,\partial/\partial\xi\right)$.

The solution to the DKE allows to calculate the neoclassical fluxes

$$\langle \boldsymbol{\Gamma}_a\cdot\nabla\psi\rangle := \left\langle \int \boldsymbol{v}_{\mathrm{m}a}\cdot\nabla\psi\ h_a\,\mathrm{d}^3\boldsymbol{v}\right\rangle,$$

$$\langle \boldsymbol{Q}_a\cdot\nabla\psi\rangle/T_a := \left\langle \int v^2/v_{\mathrm{t}a}^2\boldsymbol{v}_{\mathrm{m}a}\cdot\nabla\psi\ h_a\,\mathrm{d}^3\boldsymbol{v}\right\rangle,$$

$$\langle n_a\boldsymbol{V}_a\cdot\boldsymbol{B}\rangle/B_0 := \left\langle B/B_0\int v\xi\ h_a\,\mathrm{d}^3\boldsymbol{v}\right\rangle.$$

Transport coefficients

The source term in the DKE is

$$S_a := f_{\mathrm{M}a} \left[\frac{Bv^2}{\Omega_a} \left(s_1 A_{1a} + (v^2/v_{\mathrm{t}a}^2) s_2 A_{2a} \right) + v s_3 A_{3a} \right],$$

where $A_{1a} := n_a'/n_a - 3T_a'/2T_a - e_a E_\psi/T_a$, $A_{2a} := T_a'/T_a$, $A_{3a} := e_a B_0 \langle \boldsymbol{E} \cdot \boldsymbol{B} \rangle / T_a \left\langle B^2 \right\rangle$ are the thermodynamical forces and

The source term in the DKE is

$$S_a := f_{\mathrm{M}a}\left[\frac{Bv^2}{\Omega_a}\left(s_1 A_{1a} + (v^2/v_{\mathrm{t}a}^2) s_2 A_{2a}\right) + v s_3 A_{3a}\right],$$

where $A_{1a} := n_a'/n_a - 3T_a'/2T_a - e_a E_\psi/T_a$, $A_{2a} := T_a'/T_a$, $A_{3a} := e_a B_0 \langle \boldsymbol{E}\cdot\boldsymbol{B}\rangle / T_a \left\langle B^2 \right\rangle$ are the thermodynamical forces and

$$s_1 := -\Omega_a B^{-1} v^{-2} \boldsymbol{v}_{\mathrm{m}a}\cdot\nabla\psi, \quad s_2 := s_1, \quad s_3 := \xi B/B_0.$$

Transport coefficients

The source term in the DKE is

$$S_a := f_{\mathrm{M}a}\left[\frac{Bv^2}{\Omega_a}\left(s_1 A_{1a} + (v^2/v_{\mathrm{t}a}^2) s_2 A_{2a}\right) + v s_3 A_{3a}\right],$$

where $A_{1a} := n_a'/n_a - 3T_a'/2T_a - e_a E_\psi/T_a$, $A_{2a} := T_a'/T_a$, $A_{3a} := e_a B_0 \langle \boldsymbol{E}\cdot\boldsymbol{B}\rangle / T_a \left\langle B^2 \right\rangle$ are the thermodynamical forces and

$$s_1 := -\Omega_a B^{-1} v^{-2} \boldsymbol{v}_{\mathrm{m}a}\cdot\nabla\psi, \quad s_2 := s_1, \quad s_3 := \xi B/B_0.$$

It is convenient to use a splitting

$$h_a = f_{\mathrm{M}a}\left[\frac{Bv}{\Omega_a}\left(A_{1a} f_1 + A_{2a}(v^2/v_{\mathrm{t}a}^2) f_2\right) + A_{3a} f_3\right]$$

similar to the one used in [Beidler, NF (2011)].

Monoenergetic transport coefficients

The splitting is chosen so that $\{f_j\}_{j=1}^{3}$ are solutions to

$$\xi \boldsymbol{b} \cdot \nabla f_j + \nabla \cdot \boldsymbol{b} \frac{(1-\xi^2)}{2} \frac{\partial f_j}{\partial \xi} - \frac{\widehat{E}_\psi}{\langle B^2 \rangle} \boldsymbol{B} \times \nabla \psi \cdot \nabla f_j - \hat{\nu} \mathcal{L} f_j = s_j,$$

for $j = 1, 2, 3$, where $\hat{\nu} := \nu(v)/v$ and $\widehat{E}_\psi := E_\psi / v$.

Monoenergetic transport coefficients

The splitting is chosen so that $\{f_j\}_{j=1}^3$ are solutions to

$$\xi \boldsymbol{b} \cdot \nabla f_j + \nabla \cdot \boldsymbol{b} \frac{(1-\xi^2)}{2} \frac{\partial f_j}{\partial \xi} - \frac{\widehat{E}_\psi}{\langle B^2 \rangle} \boldsymbol{B} \times \nabla \psi \cdot \nabla f_j - \hat{\nu} \mathcal{L} f_j = s_j,$$

for $j = 1, 2, 3$, where $\hat{\nu} := \nu(v)/v$ and $\widehat{E}_\psi := E_\psi / v$.

With each solution we can compute the monoenergetic geometric coefficients

$$\widehat{D}_{ij}(\psi, v) := \left\langle \int_{-1}^{1} s_i f_j \, \mathrm{d}\xi \right\rangle, \quad i, j \in \{1, 2, 3\},$$

which for fixed $(\hat{\nu}, \widehat{E}_\psi)$ depend only on the magnetic geometry.

Monoenergetic transport coefficients

The splitting is chosen so that $\{f_j\}_{j=1}^3$ are solutions to

$$\xi \boldsymbol{b} \cdot \nabla f_j + \nabla \cdot \boldsymbol{b} \frac{(1-\xi^2)}{2} \frac{\partial f_j}{\partial \xi} - \frac{\widehat{E}_\psi}{\langle B^2 \rangle} \boldsymbol{B} \times \nabla \psi \cdot \nabla f_j - \hat{\nu} \mathcal{L} f_j = s_j,$$

for $j = 1, 2, 3$, where $\hat{\nu} := \nu(v)/v$ and $\widehat{E}_\psi := E_\psi / v$.

With each solution we can compute the monoenergetic geometric coefficients

$$\widehat{D}_{ij}(\psi, v) := \left\langle \int_{-1}^{1} s_i f_j \, \mathrm{d}\xi \right\rangle, \quad i, j \in \{1, 2, 3\},$$

which for fixed $(\hat{\nu}, \widehat{E}_\psi)$ depend only on the magnetic geometry.

At most, four of them are independent: $\{\widehat{D}_{11}, \widehat{D}_{13}, \widehat{D}_{31}, \widehat{D}_{33}\}$. For stellarator-symmetric devices or $E_\psi = 0$ we have the Onsager relation $\widehat{D}_{13} = -\widehat{D}_{31}$.

Thermal transport coefficients

Using $\widehat{D}_{ij}$, the neoclassical fluxes can be calculated using the Onsager matrix

$$\begin{bmatrix} \langle \boldsymbol{\Gamma}_a \cdot \nabla\psi \rangle \\ \langle \boldsymbol{Q}_a \cdot \nabla\psi \rangle / T_a \\ \langle n_a \boldsymbol{V}_a \cdot \boldsymbol{B} \rangle / B_0 \end{bmatrix} = \begin{bmatrix} L_{11a} & L_{12a} & L_{13a} \\ L_{21a} & L_{22a} & L_{23a} \\ L_{31a} & L_{32a} & L_{33a} \end{bmatrix} \begin{bmatrix} A_{1a} \\ A_{2a} \\ A_{3a} \end{bmatrix}.$$

Thermal transport coefficients

Using $\widehat{D}_{ij}$, the neoclassical fluxes can be calculated using the Onsager matrix

$$\begin{bmatrix} \langle \boldsymbol{\Gamma}_a \cdot \nabla\psi \rangle \\ \langle \boldsymbol{Q}_a \cdot \nabla\psi \rangle / T_a \\ \langle n_a \boldsymbol{V}_a \cdot \boldsymbol{B} \rangle / B_0 \end{bmatrix} = \begin{bmatrix} L_{11a} & L_{12a} & L_{13a} \\ L_{21a} & L_{22a} & L_{23a} \\ L_{31a} & L_{32a} & L_{33a} \end{bmatrix} \begin{bmatrix} A_{1a} \\ A_{2a} \\ A_{3a} \end{bmatrix}.$$

The thermal transport coefficients L_{ij} are integrals of the monoenergetic coefficients $\widehat{D}_{ij}$

$$L_{ija} := \int_0^\infty 2\pi v^2 f_{\mathrm{M}a} w_i w_j K_{ija} \widehat{D}_{ij} \, \mathrm{d}v \,,$$

where $w_1 = w_3 = 1$, $w_2 = v^2/v_{\mathrm{t}a}^2$ and, for each species

Thermal transport coefficients

Using $\widehat{D}_{ij}$, the neoclassical fluxes can be calculated using the Onsager matrix

$$\begin{bmatrix} \langle \boldsymbol{\Gamma}_a \cdot \nabla\psi \rangle \\ \langle \boldsymbol{Q}_a \cdot \nabla\psi \rangle / T_a \\ \langle n_a \boldsymbol{V}_a \cdot \boldsymbol{B} \rangle / B_0 \end{bmatrix} = \begin{bmatrix} L_{11a} & L_{12a} & L_{13a} \\ L_{21a} & L_{22a} & L_{23a} \\ L_{31a} & L_{32a} & L_{33a} \end{bmatrix} \begin{bmatrix} A_{1a} \\ A_{2a} \\ A_{3a} \end{bmatrix}.$$

The thermal transport coefficients L_{ij} are integrals of the monoenergetic coefficients $\widehat{D}_{ij}$

$$L_{ija} := \int_0^\infty 2\pi v^2 f_{\mathrm{M}a} w_i w_j K_{ija} \widehat{D}_{ij} \, \mathrm{d}v \, ,$$

where $w_1 = w_3 = 1$, $w_2 = v^2/v_{\mathrm{t}a}^2$ and, for each species

$$K_{ija} := -\frac{B^2 v^3}{\Omega_a^2}, \qquad i,j \in \{1,2\}; \quad K_{3ja} := \frac{Bv^2}{\Omega_a}, \quad j \in \{1,2\};$$

$$K_{i3a} := -\frac{Bv^2}{\Omega_a} = -K_{3ia}, \qquad i \in \{1,2\}; \quad K_{33a} := v.$$

Outline

Expansion in Legendre polynomials

The solution is expanded in a truncated Legendre series in ξ

$$f = \sum_{k=0}^{N_\xi} f^{(k)} P_k(\xi).$$

Expansion in Legendre polynomials

The solution is expanded in a truncated Legendre series in ξ

$$f = \sum_{k=0}^{N_\xi} f^{(k)} P_k(\xi).$$

In this basis the DKE is represented tridiagonally

$$L_k f^{(k-1)} + D_k f^{(k)} + U_k f^{(k+1)} = s^{(k)}, \quad k = 0, 1, \ldots N_\xi,$$

where $f^{(-1)} := 0$ and L_k, D_k, U_k are the linear differential operators

Expansion in Legendre polynomials

The solution is expanded in a truncated Legendre series in ξ

$$f = \sum_{k=0}^{N_\xi} f^{(k)} P_k(\xi).$$

In this basis the DKE is represented tridiagonally

$$L_k f^{(k-1)} + D_k f^{(k)} + U_k f^{(k+1)} = s^{(k)}, \quad k = 0, 1, \dots N_\xi,$$

where $f^{(-1)} := 0$ and L_k, D_k, U_k are the linear differential operators

$$L_k = \frac{k}{2k-1}\left(\boldsymbol{b}\cdot\nabla + \frac{k-1}{2}\boldsymbol{b}\cdot\nabla\ln B\right),$$

$$D_k = -\frac{\widehat{E}_\psi}{\langle B^2\rangle}\boldsymbol{B}\times\nabla\psi\cdot\nabla + \frac{k(k+1)}{2}\hat{\nu},$$

$$U_k = \frac{k+1}{2k+3}\left(\boldsymbol{b}\cdot\nabla - \frac{k+2}{2}\boldsymbol{b}\cdot\nabla\ln B\right).$$

Block Tridiagonal solution: Forward elimination

Starting from $\Delta_{N_\xi} = D_{N_\xi}$ and $\sigma^{(N_\xi)} = s^{(N_\xi)}$ we obtain recursively

$$\begin{aligned} \Delta_k &= D_k - U_k \Delta_{k+1}^{-1} L_{k+1}, \\ \sigma^{(k)} &= s^{(k)} - U_k \Delta_{k+1}^{-1} \sigma^{(k+1)}. \end{aligned}$$

for $k = N_\xi - 1, N_\xi - 2, \ldots, 0$.

Block Tridiagonal solution: Forward elimination

Starting from $\Delta_{N_\xi} = D_{N_\xi}$ and $\sigma^{(N_\xi)} = s^{(N_\xi)}$ we obtain recursively

$$\begin{aligned} \Delta_k &= D_k - U_k \Delta_{k+1}^{-1} L_{k+1}, \\ \sigma^{(k)} &= s^{(k)} - U_k \Delta_{k+1}^{-1} \sigma^{(k+1)}. \end{aligned}$$

for $k = N_\xi - 1, N_\xi - 2, \ldots, 0$. Each Δ_k and $\sigma^{(k)}$ are obtained performing Gaussian elimination over

$$\left[\begin{array}{cc|c} D_k & U_k & s^{(k)} \\ L_{k+1} & \Delta_{k+1} & \sigma^{(k+1)} \end{array}\right]$$

to eliminate U_k.

Block Tridiagonal solution: Forward elimination

Starting from $\Delta_{N_\xi} = D_{N_\xi}$ and $\sigma^{(N_\xi)} = s^{(N_\xi)}$ we obtain recursively

$$\begin{aligned}\Delta_k &= D_k - U_k \Delta_{k+1}^{-1} L_{k+1},\\ \sigma^{(k)} &= s^{(k)} - U_k \Delta_{k+1}^{-1} \sigma^{(k+1)}.\end{aligned}$$

for $k = N_\xi - 1, N_\xi - 2, \ldots, 0$. Each Δ_k and $\sigma^{(k)}$ are obtained performing Gaussian elimination over

$$\left[\begin{array}{cc|c} D_k & U_k & s^{(k)} \\ L_{k+1} & \Delta_{k+1} & \sigma^{(k+1)} \end{array}\right]$$

to eliminate U_k.

The system is factorized in a lower triangular form

$$L_k f^{(k-1)} + \Delta_k f^{(k)} = \sigma^{(k)}.$$

Block Tridiagonal solution: Backward substitution

Now is immediate to solve the factorized equation for $f^{(k)}$

$$f^{(k)} = \Delta_k^{-1}\left(\sigma^{(k)} - L_k f^{(k-1)}\right), \quad k = 0, 1, \dots, N_\xi.$$

Block Tridiagonal solution: Backward substitution

Now is immediate to solve the factorized equation for $f^{(k)}$

$$f^{(k)} = \Delta_k^{-1} \left(\sigma^{(k)} - L_k f^{(k-1)} \right), \quad k = 0, 1, \ldots, N_\xi.$$

- Discretizing the flux-surface in N_{fs} points, L_k, D_k, U_k and Δ_k are approximated by square matrices of size N_{fs}.

Block Tridiagonal solution: Backward substitution

Now is immediate to solve the factorized equation for $f^{(k)}$

$$f^{(k)} = \Delta_k^{-1}\left(\sigma^{(k)} - L_k f^{(k-1)}\right), \quad k = 0, 1, \ldots, N_\xi.$$

- Discretizing the flux-surface in N_{fs} points, L_k, D_k, U_k and Δ_k are approximated by square matrices of size N_{fs}.
- `MONKES` employs Boozer angles (θ, ζ) and a pseudospectral Fourier discretization with N_θ and N_ζ points $(N_{\text{fs}} = N_\theta N_\zeta)$.

Block Tridiagonal solution: Backward substitution

Now is immediate to solve the factorized equation for $f^{(k)}$

$$f^{(k)} = \Delta_k^{-1}\left(\sigma^{(k)} - L_k f^{(k-1)}\right), \quad k = 0, 1, \ldots, N_\xi.$$

- Discretizing the flux-surface in N_{fs} points, L_k, D_k, U_k and Δ_k are approximated by square matrices of size N_{fs}.
- `MONKES` employs Boozer angles (θ, ζ) and a pseudospectral Fourier discretization with N_θ and N_ζ points ($N_{\text{fs}} = N_\theta N_\zeta$).
- For calculating $\widehat{D}_{ij}$ only $\{f^{(k)}\}_{k=0}^{2}$ are needed. Memory required $\sim O(N_{\text{fs}}^2)$ is minimal and typically fits in a single core.

Block Tridiagonal solution: Backward substitution

Now is immediate to solve the factorized equation for $f^{(k)}$

$$f^{(k)} = \Delta_k^{-1}\left(\sigma^{(k)} - L_k f^{(k-1)}\right), \quad k = 0, 1, \dots, N_\xi.$$

- Discretizing the flux-surface in N_{fs} points, L_k, D_k, U_k and Δ_k are approximated by square matrices of size N_{fs}.
- `MONKES` employs Boozer angles (θ, ζ) and a pseudospectral Fourier discretization with N_θ and N_ζ points ($N_{\text{fs}} = N_\theta N_\zeta$).
- For calculating $\widehat{D}_{ij}$ only $\{f^{(k)}\}_{k=0}^{2}$ are needed. Memory required $\sim O(N_{\text{fs}}^2)$ is minimal and typically fits in a single core.
- The solution requires inverting $N_\xi + 1$ matrices of size N_{fs}. Arithmetical complexity $\sim O(N_{\text{fs}}^3 N_\xi)$ operations. Each inversion can be parallelized.

Block Tridiagonal solution: Backward substitution

Now is immediate to solve the factorized equation for $f^{(k)}$

$$f^{(k)} = \Delta_k^{-1}\left(\sigma^{(k)} - L_k f^{(k-1)}\right), \quad k = 0, 1, \ldots, N_\xi.$$

- Discretizing the flux-surface in N_{fs} points, L_k, D_k, U_k and Δ_k are approximated by square matrices of size N_{fs}.

- `MONKES` employs Boozer angles (θ, ζ) and a pseudospectral Fourier discretization with N_θ and N_ζ points $(N_{\text{fs}} = N_\theta N_\zeta)$.

- For calculating $\widehat{D}_{ij}$ only $\{f^{(k)}\}_{k=0}^{2}$ are needed. Memory required $\sim O(N_{\text{fs}}^2)$ is minimal and typically fits in a single core.

- The solution requires inverting $N_\xi + 1$ matrices of size N_{fs}. Arithmetical complexity $\sim O(N_{\text{fs}}^3 N_\xi)$ operations. Each inversion can be parallelized.

This algorithm allows an **accurate** calculation of the $\widehat{D}_{ij}$ at (very) low collisionality in ~ 1 minute on a single core. $\Rightarrow$ **`MONKES` is sufficiently fast for optimization purposes**.

Outline

Study cases for benchmark

Three magnetic configurations are considered. Cases with $\widehat{E}_r = 0$ are in the $1/\nu$ regime and those with $\widehat{E}_r \neq 0$ in the $\sqrt{\nu}$-ν regime.

Configuration	ψ/ψ_{lcfs}	$\hat{\nu}$ [m^{-1}]	$\widehat{E}_r$ [kV $\cdot$ s/m^2]
W7X-EIM	0.200	10^{-5}	0
W7X-EIM	0.200	10^{-5}	$3 \cdot 10^{-4}$
W7X-KJM	0.204	10^{-5}	0
W7X-KJM	0.204	10^{-5}	$3 \cdot 10^{-4}$
CIEMAT-QI4	0.250	10^{-5}	0
CIEMAT-QI4	0.250	10^{-5}	10^{-3}

Study cases for benchmark

Three magnetic configurations are considered. Cases with $\widehat{E}_r = 0$ are in the $1/\nu$ regime and those with $\widehat{E}_r \neq 0$ in the $\sqrt{\nu}$-ν regime.

Configuration	$\psi/\psi_{\mathrm{lcfs}}$	$\hat{\nu}$ [m^{-1}]	$\widehat{E}_r$ [kV $\cdot$ s/m^2]
W7X-EIM	0.200	10^{-5}	0
W7X-EIM	0.200	10^{-5}	$3 \cdot 10^{-4}$
W7X-KJM	0.204	10^{-5}	0
W7X-KJM	0.204	10^{-5}	$3 \cdot 10^{-4}$
CIEMAT-QI4	0.250	10^{-5}	0
CIEMAT-QI4	0.250	10^{-5}	10^{-3}

In order to have a typical value for `MONKES` wall-clock time, we will select resolutions $(N_\theta, N_\zeta, N_\xi)$ for which $\widehat{D}_{31}$ at low collisionality is converged up to 5–7%. This typical value of wall-clock time also gives an upper bound for the wall-clock time required for computing $\widehat{D}_{ij}$ at higher collisionalities.

Benchmark of monoenergetic coefficients

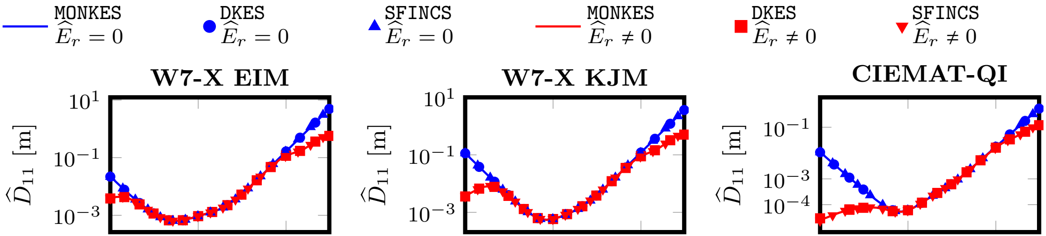

Benchmark of monoenergetic coefficients

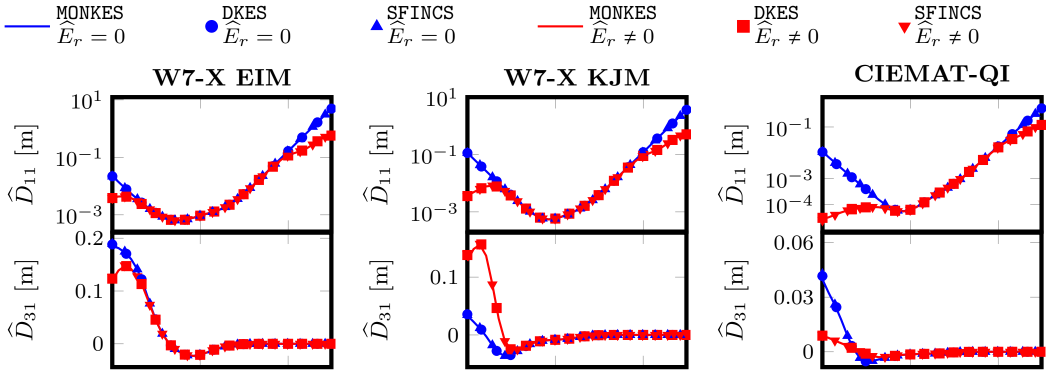

Benchmark of monoenergetic coefficients

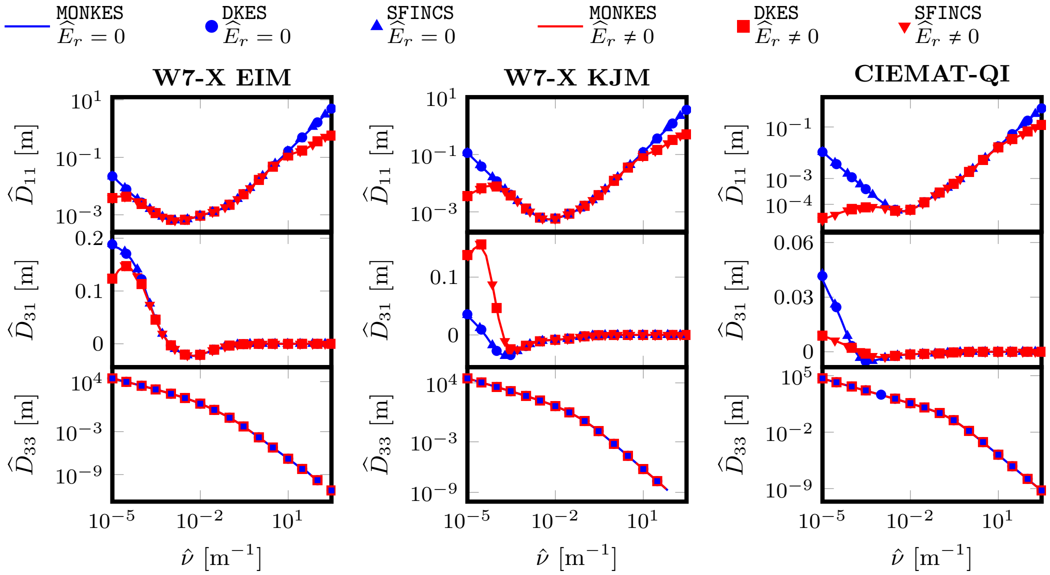

MONKES and DKES wall-clock time for the same level of relative convergence using a single core of CIEMAT's cluster.

Case	$t_{\text{clock}}^{\texttt{DKES}}$	$t_{\text{clock}}^{\texttt{MONKES}}$
W7X-EIM $\widehat{E}_r = 0$	90 s	22 s
W7X-EIM $\widehat{E}_r \neq 0$	172 s	35 s
W7X-KJM $\widehat{E}_r = 0$	698 s	31 s
W7X-KJM $\widehat{E}_r \neq 0$	421 s	47 s
CIEMAT-QI4 $\widehat{E}_r = 0$	1060 s	76 s
CIEMAT-QI4 $\widehat{E}_r \neq 0$	4990 s	76 s

MONKES and DKES wall-clock time for the same level of relative convergence using a single core of CIEMAT's cluster.

Case	$t_{\mathrm{clock}}^{\mathtt{DKES}}$	$t_{\mathrm{clock}}^{\mathtt{MONKES}}$
W7X-EIM $\widehat{E}_r = 0$	90 s	22 s
W7X-EIM $\widehat{E}_r \neq 0$	172 s	35 s
W7X-KJM $\widehat{E}_r = 0$	698 s	31 s
W7X-KJM $\widehat{E}_r \neq 0$	421 s	47 s
CIEMAT-QI4 $\widehat{E}_r = 0$	1060 s	76 s
CIEMAT-QI4 $\widehat{E}_r \neq 0$	4990 s	76 s

MONKES wall-clock time (in seconds) when running in parallel in CIEMAT's cluster.

Case \ No. cores	2	4	8	16
W7X-EIM $\widehat{E}_r = 0$	13	8	5	5
W7X-EIM $\widehat{E}_r \neq 0$	20	12	8	6
W7X-KJM $\widehat{E}_r = 0$	17	12	7	7
W7X-KJM $\widehat{E}_r \neq 0$	17	13	7	7
CIEMAT-QI4 $\widehat{E}_r = 0$	45	29	21	16
CIEMAT-QI4 $\widehat{E}_r \neq 0$	45	29	21	16

MONKES and DKES wall-clock time for the same level of relative convergence using a single core of CIEMAT's cluster.

Case	$t^{\mathtt{DKES}}_{\text{clock}}$	$t^{\mathtt{MONKES}}_{\text{clock}}$
W7X-EIM $\widehat{E}_r = 0$	90 s	22 s
W7X-EIM $\widehat{E}_r \neq 0$	172 s	35 s
W7X-KJM $\widehat{E}_r = 0$	698 s	31 s
W7X-KJM $\widehat{E}_r \neq 0$	421 s	47 s
CIEMAT-QI4 $\widehat{E}_r = 0$	1060 s	76 s
CIEMAT-QI4 $\widehat{E}_r \neq 0$	4990 s	76 s

MONKES wall-clock time (in seconds) when running in parallel in CIEMAT's cluster.

Case \ No. cores	2	4	8	16
W7X-EIM $\widehat{E}_r = 0$	13	8	5	5
W7X-EIM $\widehat{E}_r \neq 0$	20	12	8	6
W7X-KJM $\widehat{E}_r = 0$	17	12	7	7
W7X-KJM $\widehat{E}_r \neq 0$	17	13	7	7
CIEMAT-QI4 $\widehat{E}_r = 0$	45	29	21	16
CIEMAT-QI4 $\widehat{E}_r \neq 0$	45	29	21	16

MONKES is **much faster** than DKES and requires minimal memory resources. MONKES is even faster running in parallel (the CIEMAT-QI cases take 43 s on a laptop with 4 cores).

Arithmetical complexity verification: MONKES wall-clock time $\sim C_{\mathrm{alg}} N_\xi N_{\mathrm{fs}}^3$. Wall-clock times for CIEMAT's cluster cores.

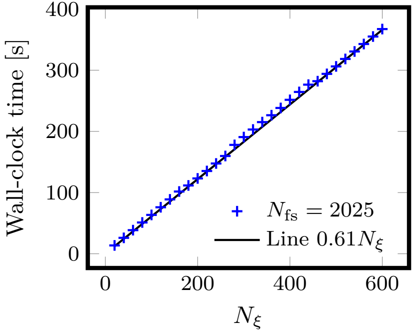

Arithmetical complexity verification: MONKES wall-clock time $\sim C_{\text{alg}} N_\xi N_{\text{fs}}^3$. Wall-clock times for CIEMAT's cluster cores.

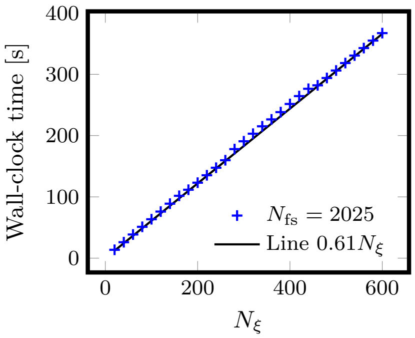

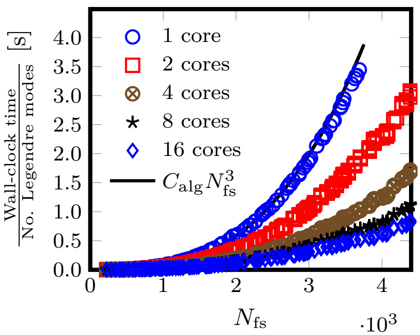

MONKES scales linearly with N_ξ and cubicly with N_{fs}. For $N_{\text{fs}} \leq 2000$ and $N_\xi \leq 200$, rapid calculations (≤ 2 minutes) on a single core.

Outline

1. Assessment of the efficiency of indirect QI optimization

In optimization, one pursues to minimize a cost function

$$\chi^2 = \sum_k \chi_k^2.$$

1. Assessment of the efficiency of indirect QI optimization

In optimization, one pursues to minimize a cost function

$$\chi^2 = \sum_k \chi_k^2.$$

- The set of proxies $\{\chi_k\}$ is selected to parametrize the desired type of stellarator. Ideally, for QI optimization $\widehat{D}_{11}, \widehat{D}_{31} \in \{\chi_k\}$ (**direct** optimization), however this was not practically feasible.

1. Assessment of the efficiency of indirect QI optimization

In optimization, one pursues to minimize a cost function

$$\chi^2 = \sum_k \chi_k^2.$$

- The set of proxies $\{\chi_k\}$ is selected to parametrize the desired type of stellarator. Ideally, for QI optimization $\widehat{D}_{11}, \widehat{D}_{31} \in \{\chi_k\}$ (**direct** optimization), however this was not practically feasible.

- **Indirect** QI optimization, **trusts** that minimizing a set of proxies $\{\chi_k\}$ which are cheap to compute, will entail a reduction of $\widehat{D}_{11}$ and $|\widehat{D}_{31}|$.

1. Assessment of the efficiency of indirect QI optimization

In optimization, one pursues to minimize a cost function

$$\chi^2 = \sum_k \chi_k^2.$$

- The set of proxies $\{\chi_k\}$ is selected to parametrize the desired type of stellarator. Ideally, for QI optimization $\widehat{D}_{11}, \widehat{D}_{31} \in \{\chi_k\}$ (**direct** optimization), however this was not practically feasible.
- **Indirect** QI optimization, **trusts** that minimizing a set of proxies $\{\chi_k\}$ which are cheap to compute, will entail a reduction of $\widehat{D}_{11}$ and $|\widehat{D}_{31}|$.
- The flat mirror [Velasco, NF (2023)] configuration CIEMAT-QI4 [Sánchez, NF (2023)] is one example of successful indirect QI optimization.

1. Assessment of the efficiency of indirect QI optimization

In optimization, one pursues to minimize a cost function

$$\chi^2 = \sum_k \chi_k^2.$$

- The set of proxies $\{\chi_k\}$ is selected to parametrize the desired type of stellarator. Ideally, for QI optimization $\widehat{D}_{11}, \widehat{D}_{31} \in \{\chi_k\}$ (**direct** optimization), however this was not practically feasible.
- **Indirect** QI optimization, **trusts** that minimizing a set of proxies $\{\chi_k\}$ which are cheap to compute, will entail a reduction of $\widehat{D}_{11}$ and $|\widehat{D}_{31}|$.
- The flat mirror [Velasco, NF (2023)] configuration CIEMAT-QI4 [Sánchez, NF (2023)] is one example of successful indirect QI optimization.

Q: Although effective, to what extent is the indirect approach efficient?

1. Assessment of the efficiency of indirect QI optimization

In optimization, one pursues to minimize a cost function

$$\chi^2 = \sum_k \chi_k^2.$$

- The set of proxies $\{\chi_k\}$ is selected to parametrize the desired type of stellarator. Ideally, for QI optimization $\widehat{D}_{11}, \widehat{D}_{31} \in \{\chi_k\}$ (**direct** optimization), however this was not practically feasible.

- **Indirect** QI optimization, **trusts** that minimizing a set of proxies $\{\chi_k\}$ which are cheap to compute, will entail a reduction of $\widehat{D}_{11}$ and $|\widehat{D}_{31}|$.

- The flat mirror [Velasco, NF (2023)] configuration CIEMAT-QI4 [Sánchez, NF (2023)] is one example of successful indirect QI optimization.

Q: Although effective, to what extent is the indirect approach efficient?

Taking advantage of `MONKES` speed of computation, we can evaluate neoclassically the large database of intermediate configurations $\sim O(10^3)$ obtained during CIEMAT-QI4 optimization campaign, to assess the efficiency of the indirect approach for minimizing $|\widehat{D}_{31}|$.

1. Assessment of the efficiency of indirect QI optimization

In order to determine the efficiency of the indirect approach we will investigate whether or not the proxies used for neoclassically optimizing CIEMAT-QI4 correlate with $|\widehat{D}_{31}|$ at $\hat{\nu} = 10^{-5}$ m^{-1} for $\widehat{E}_r = 0$ ($1/\nu$ regime) and $\widehat{E}_r \neq 0$ ($\sqrt{\nu}$-ν regime).

Proxies used for neoclassically optimizing CIEMAT-QI4:

1. Assessment of the efficiency of indirect QI optimization

In order to determine the efficiency of the indirect approach we will investigate whether or not the proxies used for neoclassically optimizing CIEMAT-QI4 correlate with $|\widehat{D}_{31}|$ at $\hat{\nu} = 10^{-5}\ \mathrm{m}^{-1}$ for $\widehat{E}_r = 0$ ($1/\nu$ regime) and $\widehat{E}_r \neq 0$ ($\sqrt{\nu}$-ν regime).

Proxies used for neoclassically optimizing CIEMAT-QI4:

- $\epsilon_{\mathrm{eff}} \equiv$ Effective ripple. Encapsulates radial transport in the $1/\nu$.

1. Assessment of the efficiency of indirect QI optimization

In order to determine the efficiency of the indirect approach we will investigate whether or not the proxies used for neoclassically optimizing CIEMAT-QI4 correlate with $|\widehat{D}_{31}|$ at $\hat{\nu} = 10^{-5}\ \mathrm{m}^{-1}$ for $\widehat{E}_r = 0$ ($1/\nu$ regime) and $\widehat{E}_r \neq 0$ ($\sqrt{\nu}$-ν regime).

Proxies used for neoclassically optimizing CIEMAT-QI4:

- $\epsilon_{\mathrm{eff}} \equiv$ Effective ripple. Encapsulates radial transport in the $1/\nu$.
- $\sigma^2\left(B^{\mathrm{r}}_{\mathrm{min}}\right) \equiv$ Variance of the relative minima of B on the flux-surface.

1. Assessment of the efficiency of indirect QI optimization

In order to determine the efficiency of the indirect approach we will investigate whether or not the proxies used for neoclassically optimizing CIEMAT-QI4 correlate with $|\widehat{D}_{31}|$ at $\hat{\nu} = 10^{-5}\ \mathrm{m}^{-1}$ for $\widehat{E}_r = 0$ ($1/\nu$ regime) and $\widehat{E}_r \neq 0$ ($\sqrt{\nu}$-ν regime).

Proxies used for neoclassically optimizing CIEMAT-QI4:

- $\epsilon_{\mathrm{eff}} \equiv$ Effective ripple. Encapsulates radial transport in the $1/\nu$.
- $\sigma^2\left(B^{\mathrm{r}}_{\mathrm{min}}\right) \equiv$ Variance of the relative minima of B on the flux-surface.
- $\Gamma_{\mathrm{c}} \equiv$ Measures the deviation of constant $J = \oint v_{\|}\,\mathrm{d}l$ regions from flux-surfaces [Nemov, PoP (2008)]. In an omnigenous stellarator $J = J(\psi)$.

1. Assessment of the efficiency of indirect QI optimization

In order to determine the efficiency of the indirect approach we will investigate whether or not the proxies used for neoclassically optimizing CIEMAT-QI4 correlate with $|\widehat{D}_{31}|$ at $\hat{\nu} = 10^{-5}\ \mathrm{m}^{-1}$ for $\widehat{E}_r = 0$ ($1/\nu$ regime) and $\widehat{E}_r \neq 0$ ($\sqrt{\nu}$-ν regime).

Proxies used for neoclassically optimizing CIEMAT-QI4:

- $\epsilon_{\mathrm{eff}} \equiv$ Effective ripple. Encapsulates radial transport in the $1/\nu$.
- $\sigma^2\left(B^{\mathrm{r}}_{\mathrm{min}}\right) \equiv$ Variance of the relative minima of B on the flux-surface.
- $\Gamma_{\mathrm{c}} \equiv$ Measures the deviation of constant $J = \oint v_{\|}\, \mathrm{d}l$ regions from flux-surfaces [Nemov, PoP (2008)]. In an omnigenous stellarator $J = J(\psi)$.
- $\Gamma_{\alpha} \equiv$ Measures the deviation of constant J regions from being closed surfaces [Velasco, NF (2021)].

1. Assessment of the efficiency of indirect QI optimization

In order to determine the efficiency of the indirect approach we will investigate whether or not the proxies used for neoclassically optimizing CIEMAT-QI4 correlate with $|\widehat{D}_{31}|$ at $\hat{\nu} = 10^{-5}\ \mathrm{m}^{-1}$ for $\widehat{E}_r = 0$ ($1/\nu$ regime) and $\widehat{E}_r \neq 0$ ($\sqrt{\nu}$-ν regime).

Proxies used for neoclassically optimizing CIEMAT-QI4:

- $\epsilon_{\mathrm{eff}} \equiv$ Effective ripple. Encapsulates radial transport in the $1/\nu$.
- $\sigma^2\left(B^{\mathrm{r}}_{\mathrm{min}}\right) \equiv$ Variance of the relative minima of B on the flux-surface.
- $\Gamma_{\mathrm{c}} \equiv$ Measures the deviation of constant $J = \oint v_{\parallel}\, \mathrm{d}l$ regions from flux-surfaces [Nemov, PoP (2008)]. In an omnigenous stellarator $J = J(\psi)$.
- $\Gamma_{\alpha} \equiv$ Measures the deviation of constant J regions from being closed surfaces [Velasco, NF (2021)].

Vanish for an omnigenous magnetic field

1. Assessment of the efficiency of indirect QI optimization

In order to determine the efficiency of the indirect approach we will investigate whether or not the proxies used for neoclassically optimizing CIEMAT-QI4 correlate with $|\widehat{D}_{31}|$ at $\hat{\nu} = 10^{-5}\ \mathrm{m}^{-1}$ for $\widehat{E}_r = 0$ ($1/\nu$ regime) and $\widehat{E}_r \neq 0$ ($\sqrt{\nu}$-ν regime).

Proxies used for neoclassically optimizing CIEMAT-QI4:

- $\epsilon_{\mathrm{eff}} \equiv$ Effective ripple. Encapsulates radial transport in the $1/\nu$.
- $\sigma^2\left(B^{\mathrm{r}}_{\mathrm{min}}\right) \equiv$ Variance of the relative minima of B on the flux-surface.
- $\Gamma_c \equiv$ Measures the deviation of constant $J = \oint v_{\|}\,\mathrm{d}l$ regions from flux-surfaces [Nemov, PoP (2008)]. In an omnigenous stellarator $J = J(\psi)$.
- $\Gamma_\alpha \equiv$ Measures the deviation of constant J regions from being closed surfaces [Velasco, NF (2021)].

Vanish for an omnigenous magnetic field

- $\sigma^2\left(B(\theta, 0)\right) \equiv$ Variance of B at the (poloidally closed) line $\zeta = 0$.

1. Assessment of the efficiency of indirect QI optimization

In order to determine the efficiency of the indirect approach we will investigate whether or not the proxies used for neoclassically optimizing CIEMAT-QI4 correlate with $|\widehat{D}_{31}|$ at $\hat{\nu} = 10^{-5}$ m^{-1} for $\widehat{E}_r = 0$ ($1/\nu$ regime) and $\widehat{E}_r \neq 0$ ($\sqrt{\nu}$-ν regime).

Proxies used for neoclassically optimizing CIEMAT-QI4:

- $\epsilon_{\mathrm{eff}} \equiv$ Effective ripple. Encapsulates radial transport in the $1/\nu$.
- $\sigma^2\left(B^{\mathrm{r}}_{\mathrm{min}}\right) \equiv$ Variance of the relative minima of B on the flux-surface.
- $\Gamma_{\mathrm{c}} \equiv$ Measures the deviation of constant $J = \oint v_{\|}\,\mathrm{d}l$ regions from flux-surfaces [Nemov, PoP (2008)]. In an omnigenous stellarator $J = J(\psi)$.
- $\Gamma_{\alpha} \equiv$ Measures the deviation of constant J regions from being closed surfaces [Velasco, NF (2021)].

Vanish for an omnigenous magnetic field

- $\sigma^2\left(B(\theta,0)\right) \equiv$ Variance of B at the (poloidally closed) line $\zeta = 0$.

Vanishes for a QI magnetic field

In the $1/\nu$ regime ($\widehat{E}_r = 0$) $\widehat{D}_{11} \propto \epsilon_{\text{eff}}^{3/2}$. Its value is often used as an indicator of overall (radial) neoclassical optimization.

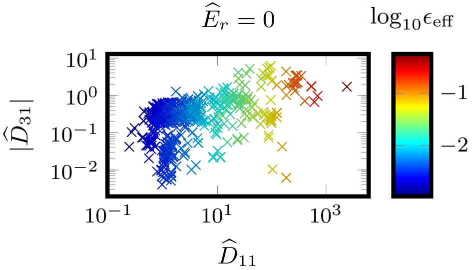

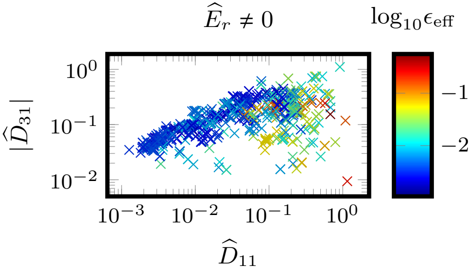

1. Assessment of the efficiency of indirect QI optimization: effective ripple ϵ_{eff}

In the $1/\nu$ regime ($\widehat{E}_r = 0$) $\widehat{D}_{11} \propto \epsilon_{\text{eff}}^{3/2}$. Its value is often used as an indicator of overall (radial) neoclassical optimization.

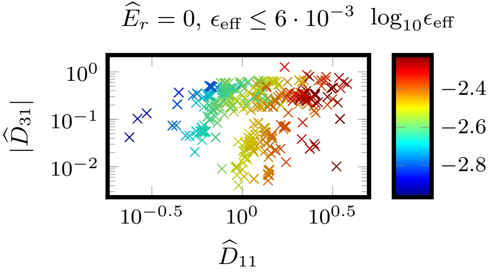

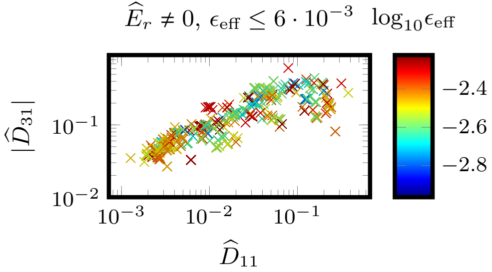

In the $1/\nu$ regime ($\widehat{E}_r = 0$) $\widehat{D}_{11} \propto \epsilon_{\text{eff}}^{3/2}$. Its value is often used as an indicator of overall (radial) neoclassical optimization.

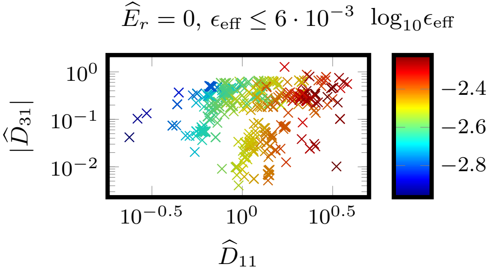

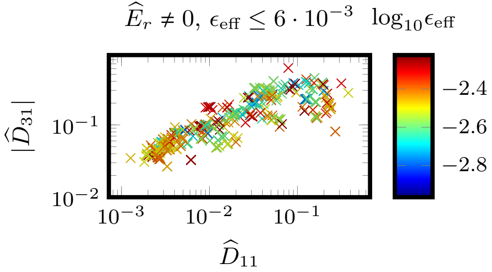

- For $\widehat{E}_r = 0$ (left), those configurations with low levels of radial transport can have large bootstrap current.

In the $1/\nu$ regime ($\widehat{E}_r = 0$) $\widehat{D}_{11} \propto \epsilon_{\text{eff}}^{3/2}$. Its value is often used as an indicator of overall (radial) neoclassical optimization.

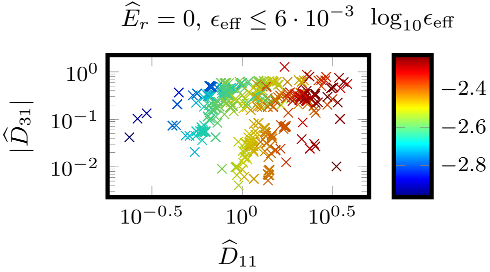

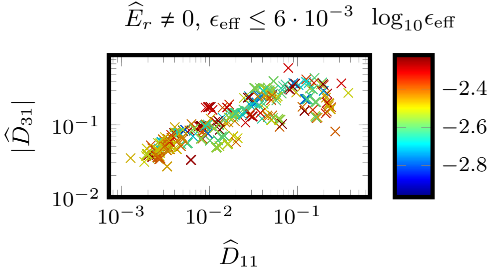

- For $\widehat{E}_r = 0$ (left), those configurations with low levels of radial transport can have large bootstrap current. There seems to be a trade-off between $\widehat{D}_{11}$ and $|\widehat{D}_{31}|$ for sufficiently small ϵ_{eff}.

In the $1/\nu$ regime ($\widehat{E}_r = 0$) $\widehat{D}_{11} \propto \epsilon_{\text{eff}}^{3/2}$. Its value is often used as an indicator of overall (radial) neoclassical optimization.

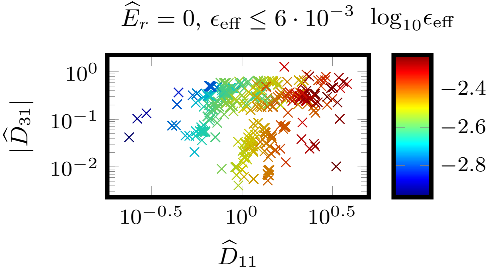

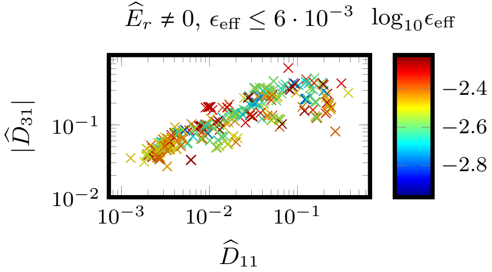

- For $\widehat{E}_r = 0$ (left), those configurations with low levels of radial transport can have large bootstrap current. There seems to be a trade-off between $\widehat{D}_{11}$ and $|\widehat{D}_{31}|$ for sufficiently small ϵ_{eff}.
- For $\widehat{E}_r \neq 0$ (right) and sufficiently small ϵ_{eff}, those configurations with low $\widehat{D}_{11}$ also have small $\widehat{D}_{31}$.

1. Assessment of the efficiency of indirect QI optimization: effective ripple ϵ_{eff}

In the $1/\nu$ regime ($\widehat{E}_r = 0$) $\widehat{D}_{11} \propto \epsilon_{\text{eff}}^{3/2}$. Its value is often used as an indicator of overall (radial) neoclassical optimization.

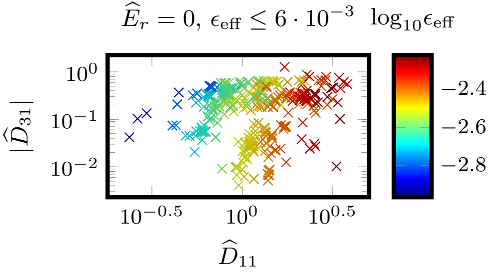

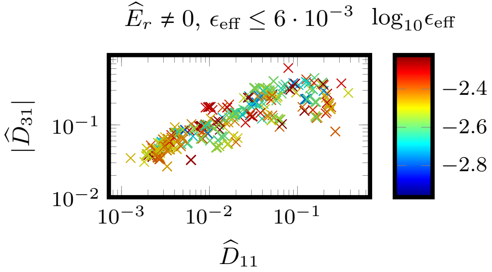

- For $\widehat{E}_r = 0$ (left), those configurations with low levels of radial transport can have large bootstrap current. There seems to be a trade-off between $\widehat{D}_{11}$ and $|\widehat{D}_{31}|$ for sufficiently small ϵ_{eff}.
- For $\widehat{E}_r \neq 0$ (right) and sufficiently small ϵ_{eff}, those configurations with low $\widehat{D}_{11}$ also have small $\widehat{D}_{31}$. There seems to be a correlation between $\widehat{D}_{11}$ and $\widehat{D}_{31}$.

1. Assessment of the efficiency of indirect QI optimization: variance of relative minima

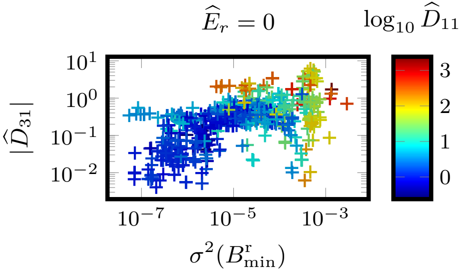

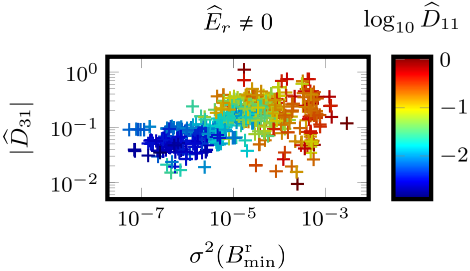

1. Assessment of the efficiency of indirect QI optimization: variance of relative minima

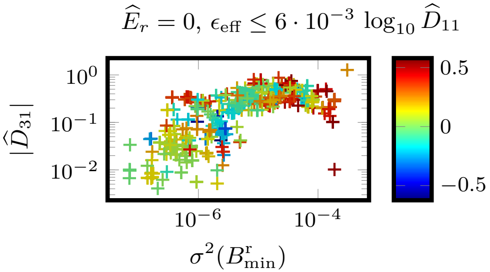

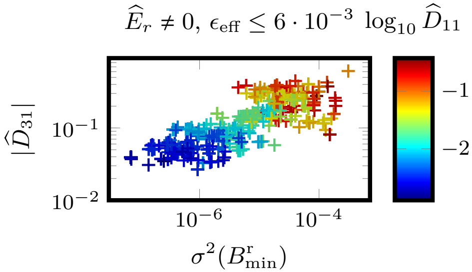

1. Assessment of the efficiency of indirect QI optimization: variance of relative minima

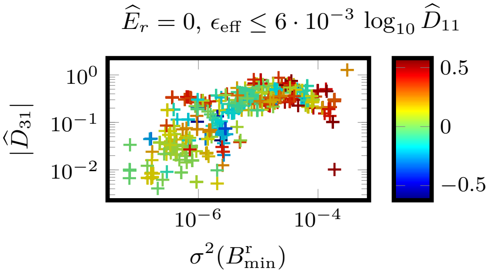

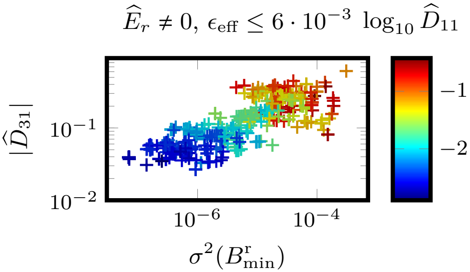

- For $\widehat{E}_r = 0$ (left) minimizing the variance is inefficient. For $\sigma^2(B^{\rm r}_{\rm min}) \sim 1 \cdot 10^{-6}$, $|\widehat{D}_{31}|$ can vary almost 2 orders of magnitude.

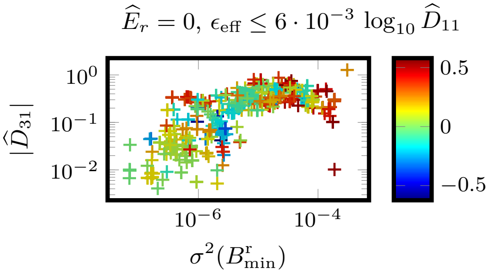

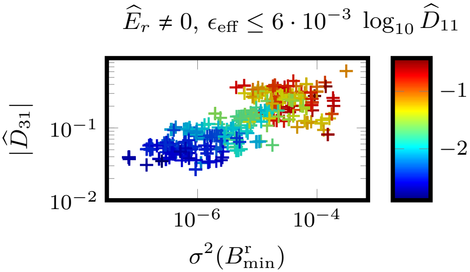

- For $\widehat{E}_r = 0$ (left) minimizing the variance is inefficient. For $\sigma^2(B^{\rm r}_{\rm min}) \sim 1 \cdot 10^{-6}$, $|\widehat{D}_{31}|$ can vary almost 2 orders of magnitude.
- For $\widehat{E}_r \neq 0$ (right), moderate correlation between $\sigma^2(B^{\rm r}_{\rm min})$ and $\widehat{D}_{11}$ and between $\sigma^2(B^{\rm r}_{\rm min})$ and $|\widehat{D}_{31}|$ is observed. Still not very efficient.

1. Assessment of the efficiency of indirect QI optimization: fast ion proxies

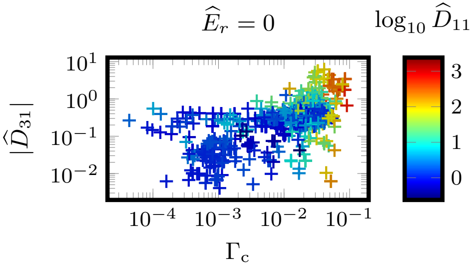

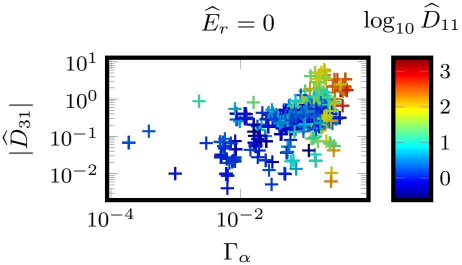

1. Assessment of the efficiency of indirect QI optimization: fast ion proxies

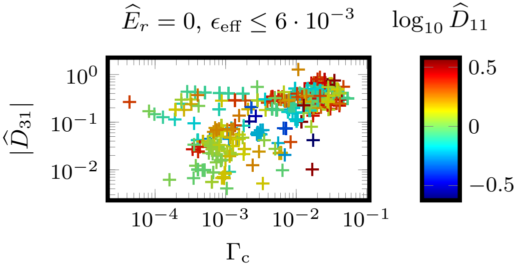

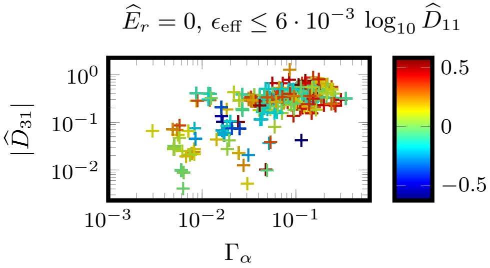

- For $\widehat{E}_r = 0$, almost no correlation between Γ_c (left) and $|\widehat{D}_{31}|$. Slightly better for Γ_α (right).

1. Assessment of the efficiency of indirect QI optimization: fast ion proxies

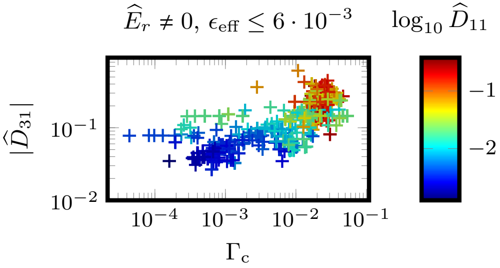

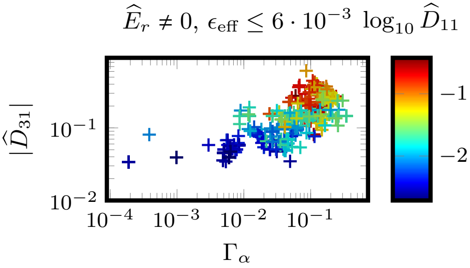

- For $\widehat{E}_r = 0$, almost no correlation between Γ_c (left) and $|\widehat{D}_{31}|$. Slightly better for Γ_α (right).
- For $\widehat{E}_r \neq 0$ the conclusion is similar but with stronger correlation for both Γ_c (left) and Γ_α (right).

1. Assessment of the efficiency of indirect QI optimization: fast ion proxies

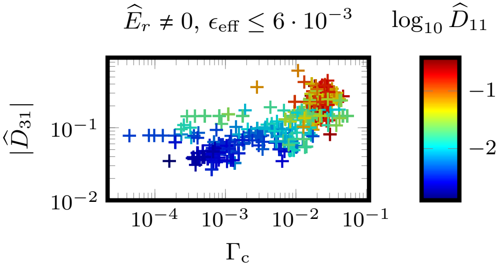

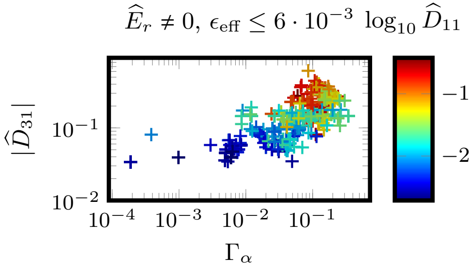

- For $\widehat{E}_r = 0$, almost no correlation between Γ_c (left) and $|\widehat{D}_{31}|$. Slightly better for Γ_α (right).
- For $\widehat{E}_r \neq 0$ the conclusion is similar but with stronger correlation for both Γ_c (left) and Γ_α (right).

Numerical results suggest that Γ_α allows slightly better trade-off to minimize $|\widehat{D}_{31}|$ than Γ_c.

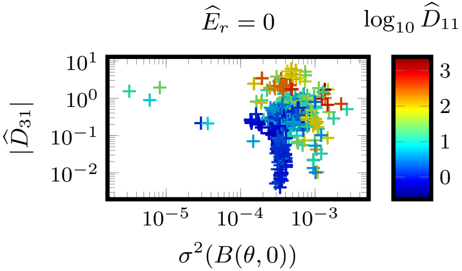
$\widehat{E}_r = 0$
$\log_{10} \widehat{D}_{11}$
$|\widehat{D}_{31}|$
10^1
10^0
10^{-1}
10^{-2}
10^{-5}
10^{-4}
10^{-3}
$\sigma^2(B(\theta,0))$
3
2
1
0

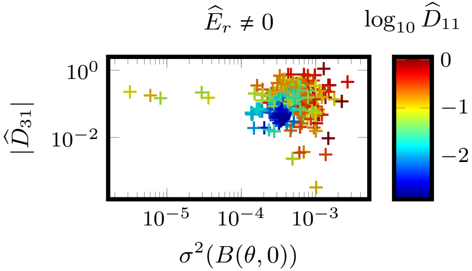
$\widehat{E}_r \neq 0$
$\log_{10} \widehat{D}_{11}$
$|\widehat{D}_{31}|$
10^0
10^{-2}
10^{-5}
10^{-4}
10^{-3}
$\sigma^2(B(\theta,0))$
0
-1
-2

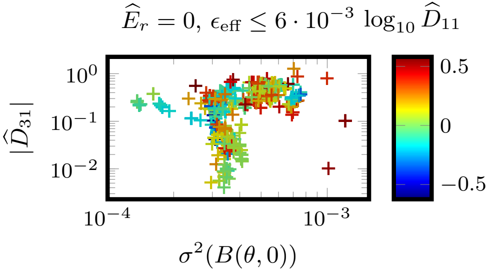

$\widehat{E}_r = 0,\ \epsilon_{\rm eff} \leq 6 \cdot 10^{-3}\ \log_{10} \widehat{D}_{11}$
$|\widehat{D}_{31}|$
10^0
10^{-1}
10^{-2}
10^{-4}
10^{-3}
$\sigma^2(B(\theta, 0))$
0.5
0
−0.5

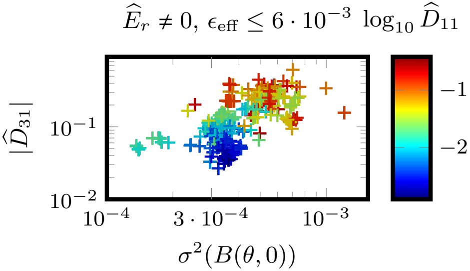

$\widehat{E}_r \neq 0,\ \epsilon_{\rm eff} \leq 6 \cdot 10^{-3}\ \log_{10} \widehat{D}_{11}$
$|\widehat{D}_{31}|$
10^{-1}
10^{-2}
10^{-4}
$3 \cdot 10^{-4}$
10^{-3}
$\sigma^2(B(\theta, 0))$
−1
−2

1. Assessment of the efficiency of indirect QI optimization: poloidally closed maximum

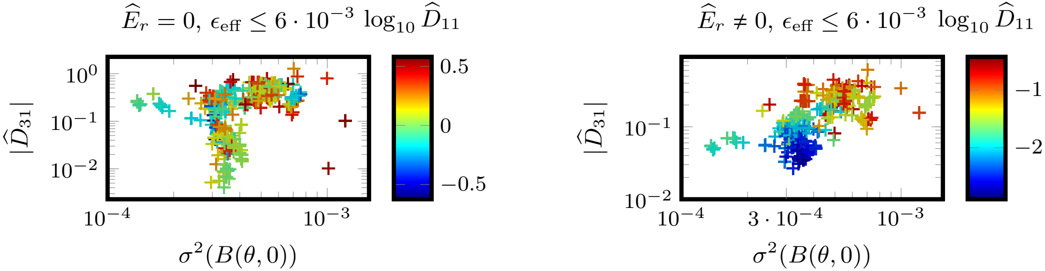

- For $\widehat{E}_r = 0$, no correlation is observed between $\sigma^2(B(\theta,0))$ and $|\widehat{D}_{31}|$.

1. Assessment of the efficiency of indirect QI optimization: poloidally closed maximum

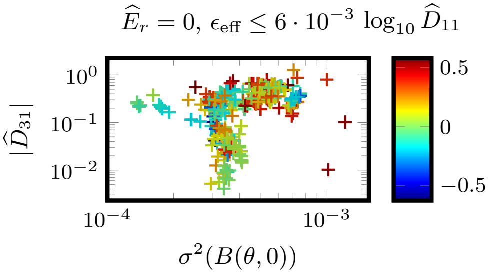

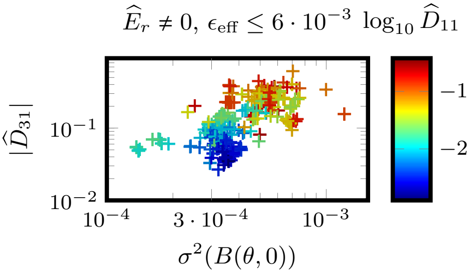

- For $\widehat{E}_r = 0$, no correlation is observed between $\sigma^2(B(\theta, 0))$ and $|\widehat{D}_{31}|$.
- For $\widehat{E}_r \neq 0$, weak correlation. At $\sigma^2(B(\theta, 0)) \sim 3 \cdot 10^{-4}$, $|\widehat{D}_{31}|$ can vary almost 1 order of magnitude.

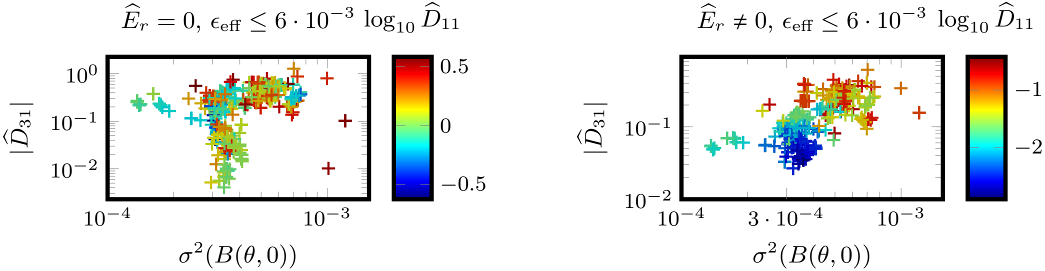

- For $\widehat{E}_r = 0$, no correlation is observed between $\sigma^2(B(\theta, 0))$ and $|\widehat{D}_{31}|$.
- For $\widehat{E}_r \neq 0$, weak correlation. At $\sigma^2(B(\theta, 0)) \sim 3 \cdot 10^{-4}$, $|\widehat{D}_{31}|$ can vary almost 1 order of magnitude.

The indirect approach is not efficient for reducing the bootstrap current, specially for $\widehat{E}_r = 0$.

1. Assessment of the efficiency of indirect QI optimization: poloidally closed maximum

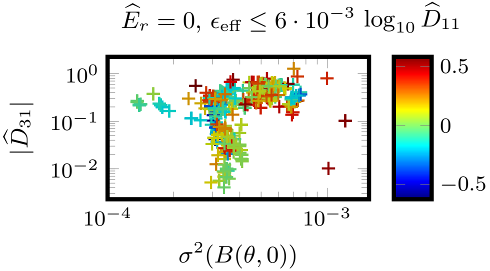

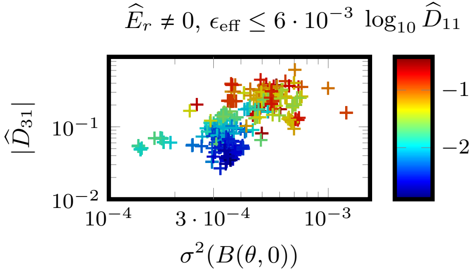

- For $\widehat{E}_r = 0$, no correlation is observed between $\sigma^2(B(\theta, 0))$ and $|\widehat{D}_{31}|$.
- For $\widehat{E}_r \neq 0$, weak correlation. At $\sigma^2(B(\theta, 0)) \sim 3 \cdot 10^{-4}$, $|\widehat{D}_{31}|$ can vary almost 1 order of magnitude.

The indirect approach is not efficient for reducing the bootstrap current, specially for $\widehat{E}_r = 0$. **Can we do better?** Hopefully, **direct optimization** of the $|\widehat{D}_{31}|$ coefficient will improve this efficiency.

2. Computing derivatives of $\widehat{D}_{ij}$ using `MONKES`

Let $\eta \in \{B_{mn}, \widehat{E}_\psi, \hat{\nu}, \iota, B_\theta, B_\zeta, \ldots\}$ be a parameter upon which the DKE depends. For gradient-based optimization methods it is useful to compute

$$\frac{\partial \widehat{D}_{ij}}{\partial \eta} = \left\langle \int_{-1}^{1} s_i \frac{\partial f_j}{\partial \eta} \, \mathrm{d}\xi \right\rangle + \left\langle \frac{V'}{\sqrt{g}} \int_{-1}^{1} \frac{\partial}{\partial \eta} \left(\frac{\sqrt{g} s_i}{V'} \right) f_j \, \mathrm{d}\xi \right\rangle.$$

2. Computing derivatives of $\widehat{D}_{ij}$ using `MONKES`

Let $\eta \in \{B_{mn}, \widehat{E}_\psi, \hat{\nu}, \iota, B_\theta, B_\zeta, \ldots\}$ be a parameter upon which the DKE depends. For gradient-based optimization methods it is useful to compute

$$\frac{\partial \widehat{D}_{ij}}{\partial \eta} = \left\langle \int_{-1}^{1} s_i \frac{\partial f_j}{\partial \eta} \, \mathrm{d}\xi \right\rangle + \left\langle \frac{V'}{\sqrt{g}} \int_{-1}^{1} \frac{\partial}{\partial \eta} \left(\frac{\sqrt{g} s_i}{V'} \right) f_j \, \mathrm{d}\xi \right\rangle.$$

Let f_j and g_i be, respectively, the solutions to the DKE and its adjoint [Paul, JPP (2020)]

$$\begin{aligned} \mathcal{V} f_j - \hat{\nu} \mathcal{L} f_j &= s_j, \\ -\mathcal{V} g_i - \hat{\nu} \mathcal{L} g_i &= s_i, \end{aligned}$$

where $\mathcal{V} := \xi \boldsymbol{b} \cdot \nabla + \nabla \cdot \boldsymbol{b}(1 - \xi^2)/2 \, \partial/\partial \xi - \widehat{E}_\psi / \langle B^2 \rangle \boldsymbol{B} \times \nabla \psi \cdot \nabla$.

2. Computing derivatives of $\widehat{D}_{ij}$ using `MONKES`

Let $\eta \in \{B_{mn}, \widehat{E}_\psi, \hat{\nu}, \iota, B_\theta, B_\zeta, \ldots\}$ be a parameter upon which the DKE depends. For gradient-based optimization methods it is useful to compute

$$\frac{\partial \widehat{D}_{ij}}{\partial \eta} = \left\langle \int_{-1}^{1} s_i \frac{\partial f_j}{\partial \eta} \, \mathrm{d}\xi \right\rangle + \left\langle \frac{V'}{\sqrt{g}} \int_{-1}^{1} \frac{\partial}{\partial \eta} \left(\frac{\sqrt{g} s_i}{V'} \right) f_j \, \mathrm{d}\xi \right\rangle.$$

Let f_j and g_i be, respectively, the solutions to the DKE and its adjoint [Paul, JPP (2020)]

$$\mathcal{V} f_j - \hat{\nu} \mathcal{L} f_j = s_j,$$
$$-\mathcal{V} g_i - \hat{\nu} \mathcal{L} g_i = s_i,$$

where $\mathcal{V} := \xi \boldsymbol{b} \cdot \nabla + \nabla \cdot \boldsymbol{b} (1 - \xi^2)/2 \, \partial/\partial \xi - \widehat{E}_\psi / \langle B^2 \rangle \boldsymbol{B} \times \nabla \psi \cdot \nabla$.

We can compute the difficult part of $\partial \widehat{D}_{ij}/\partial \eta$ using the adjoint solution g_i as

$$\left\langle \int_{-1}^{1} s_i \frac{\partial f_j}{\partial \eta} \, \mathrm{d}\xi \right\rangle = \left\langle \int_{-1}^{1} \frac{\partial s_j}{\partial \eta} g_i \, \mathrm{d}\xi \right\rangle - \left\langle \int_{-1}^{1} g_i \mathcal{V}_\eta f_j \, \mathrm{d}\xi \right\rangle + \frac{\partial \hat{\nu}}{\partial \eta} \left\langle \int_{-1}^{1} g_i \mathcal{L} f_j \, \mathrm{d}\xi \right\rangle.$$

where $\mathcal{V}_\eta$ is the differential operator whose coefficients are the derivatives of those of $\mathcal{V}$, i.e.

$$\mathcal{V}_\eta f_j := \frac{\partial}{\partial \eta} \mathcal{V} f_j - \mathcal{V} \frac{\partial}{\partial \eta} f_j.$$

2. Computing derivatives of $\widehat{D}_{ij}$ using MONKES

An adjoint method for computing $\partial \widehat{D}_{ij} / \partial \eta$ has been implemented in `MONKES` .

2. Computing derivatives of $\widehat{D}_{ij}$ using MONKES

An adjoint method for computing $\partial\widehat{D}_{ij}/\partial\eta$ has been implemented in MONKES .

- The opposite of the adjoint solution $-g_i$ can be obtained as the solution to the DKE for $\hat{\nu} \mapsto -\hat{\nu}$.

2. Computing derivatives of $\widehat{D}_{ij}$ using MONKES

An adjoint method for computing $\partial\widehat{D}_{ij}/\partial\eta$ has been implemented in `MONKES` .

- The opposite of the adjoint solution $-g_i$ can be obtained as the solution to the DKE for $\hat{\nu} \mapsto -\hat{\nu}$.

- At the computational cost of solving twice the DKE (and some extra matrix-vector products) we can compute all the required derivatives.

2. Computing derivatives of $\widehat{D}_{ij}$ using MONKES

An adjoint method for computing $\partial \widehat{D}_{ij} / \partial \eta$ has been implemented in **MONKES** .

- The opposite of the adjoint solution $-g_i$ can be obtained as the solution to the DKE for $\hat{\nu} \mapsto -\hat{\nu}$.
- At the computational cost of solving twice the DKE (and some extra matrix-vector products) we can compute all the required derivatives.

Example of scan over B_{01} (Boozer) Fourier mode for W7-X EIM at $\hat{\nu} = 10^{-5}$ m^{-1}.

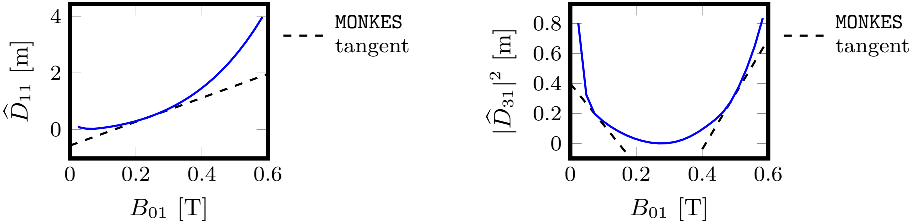

2. Computing derivatives of $\widehat{D}_{ij}$ using MONKES

An adjoint method for computing $\partial\widehat{D}_{ij}/\partial\eta$ has been implemented in **MONKES** .

- The opposite of the adjoint solution $-g_i$ can be obtained as the solution to the DKE for $\hat{\nu} \mapsto -\hat{\nu}$.

- At the computational cost of solving twice the DKE (and some extra matrix-vector products) we can compute all the required derivatives.

Example of scan over B_{01} (Boozer) Fourier mode for W7-X EIM at $\hat{\nu} = 10^{-5}$ m^{-1}.

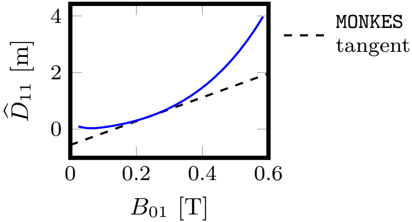

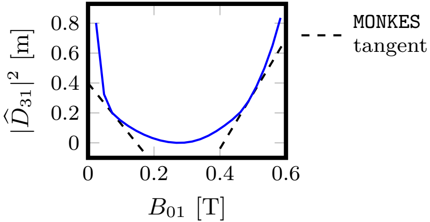

MONKES can also provide calculations of the derivatives of the monoenergetic coefficients.

3. Exploring pwO configuration space: from pwO to QI

Direct optimization of fast-ion confinement [Bindel, JPP (2023)] has inspired a new ideal design goal: piecewise omnigeneity (pwO) [Velasco, arXiv (2024)].

3. Exploring pwO configuration space: from pwO to QI

Direct optimization of fast-ion confinement [Bindel, JPP (2023)] has inspired a new ideal design goal: piecewise omnigeneity (pwO) [Velasco, arXiv (2024)]. In a pwO magnetic field, $J = \oint v_{\|} \, \mathrm{d}l$ is a flux-function **piecewisely**.

Direct optimization of fast-ion confinement [Bindel, JPP (2023)] has inspired a new ideal design goal: piecewise omnigeneity (pwO) [Velasco, arXiv (2024)]. In a pwO magnetic field, $J = \oint v_\parallel \, \mathrm{d}l$ is a flux-function **piecewisely**. A simple pwO magnetic field is given by

$$B(\theta,\zeta) \sim B_{\min} + (B_{\max} - B_{\min}) \exp\left(- \left(\frac{\theta - t_\zeta \zeta}{w_\theta} \right)^{2p} - \left(\frac{\zeta}{w_\zeta} \right)^{2p} \right), \qquad \iota = -t_\zeta \frac{w_\zeta N_{\mathrm{fp}}}{\pi - w_\zeta N_{\mathrm{fp}}}$$

in the limit $p \to \infty$. For $w_\theta/\pi > 1$, the field becomes nearly QI. Example with $p = 10$.

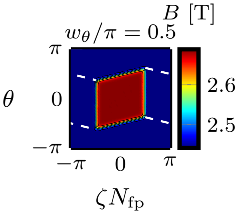

3. Exploring pwO configuration space: from pwO to QI

Direct optimization of fast-ion confinement [Bindel, JPP (2023)] has inspired a new ideal design goal: piecewise omnigeneity (pwO) [Velasco, arXiv (2024)]. In a pwO magnetic field, $J = \oint v_\parallel \, \mathrm{d}l$ is a flux-function **piecewisely**. A simple pwO magnetic field is given by

$$B(\theta,\zeta) \sim B_{\min} + (B_{\max} - B_{\min}) \exp\left(-\left(\frac{\theta - t_\zeta \zeta}{w_\theta}\right)^{2p} - \left(\frac{\zeta}{w_\zeta}\right)^{2p} \right), \qquad \iota = -t_\zeta \frac{w_\zeta N_{\mathrm{fp}}}{\pi - w_\zeta N_{\mathrm{fp}}}$$

in the limit $p \to \infty$. For $w_\theta/\pi > 1$, the field becomes nearly QI. Example with $p = 10$.

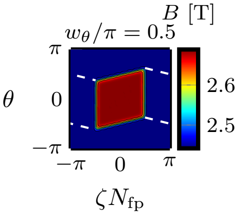

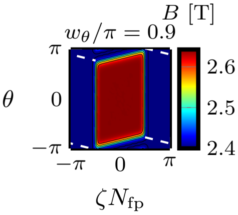

3. Exploring pwO configuration space: from pwO to QI

Direct optimization of fast-ion confinement [Bindel, JPP (2023)] has inspired a new ideal design goal: piecewise omnigeneity (pwO) [Velasco, arXiv (2024)]. In a pwO magnetic field, $J = \oint v_\parallel \, \mathrm{d}l$ is a flux-function **piecewisely**. A simple pwO magnetic field is given by

$$B(\theta,\zeta) \sim B_{\min} + (B_{\max} - B_{\min}) \exp\left(-\left(\frac{\theta - t_\zeta \zeta}{w_\theta}\right)^{2p} - \left(\frac{\zeta}{w_\zeta}\right)^{2p} \right), \qquad \iota = -t_\zeta \frac{w_\zeta N_{\mathrm{fp}}}{\pi - w_\zeta N_{\mathrm{fp}}}$$

in the limit $p \to \infty$. For $w_\theta/\pi > 1$, the field becomes nearly QI. Example with $p = 10$.

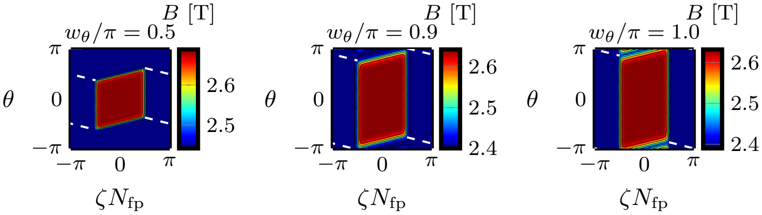

3. Exploring pwO configuration space: from pwO to QI

Direct optimization of fast-ion confinement [Bindel, JPP (2023)] has inspired a new ideal design goal: piecewise omnigeneity (pwO) [Velasco, arXiv (2024)]. In a pwO magnetic field, $J = \oint v_\parallel \, \mathrm{d}l$ is a flux-function **piecewisely**. A simple pwO magnetic field is given by

$$B(\theta,\zeta) \sim B_{\min} + (B_{\max} - B_{\min}) \exp\left(- \left(\frac{\theta - t_\zeta \zeta}{w_\theta}\right)^{2p} - \left(\frac{\zeta}{w_\zeta}\right)^{2p} \right), \qquad \iota = -t_\zeta \frac{w_\zeta N_{\mathrm{fp}}}{\pi - w_\zeta N_{\mathrm{fp}}}$$

in the limit $p \to \infty$. For $w_\theta/\pi > 1$, the field becomes nearly QI. Example with $p = 10$.

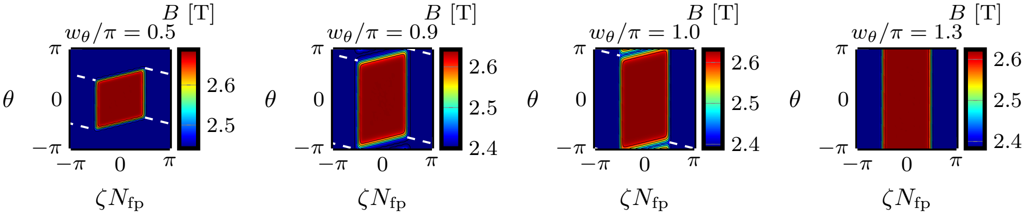

3. Exploring pwO configuration space: from pwO to QI

Direct optimization of fast-ion confinement [Bindel, JPP (2023)] has inspired a new ideal design goal: piecewise omnigeneity (pwO) [Velasco, arXiv (2024)]. In a pwO magnetic field, $J = \oint v_\parallel \, \mathrm{d}l$ is a flux-function **piecewisely**. A simple pwO magnetic field is given by

$$B(\theta,\zeta) \sim B_{\min} + (B_{\max} - B_{\min}) \exp\left(- \left(\frac{\theta - t_\zeta \zeta}{w_\theta}\right)^{2p} - \left(\frac{\zeta}{w_\zeta}\right)^{2p} \right), \qquad \iota = -t_\zeta \frac{w_\zeta N_{\mathrm{fp}}}{\pi - w_\zeta N_{\mathrm{fp}}}$$

in the limit $p \to \infty$. For $w_\theta/\pi > 1$, the field becomes nearly QI. Example with $p = 10$.

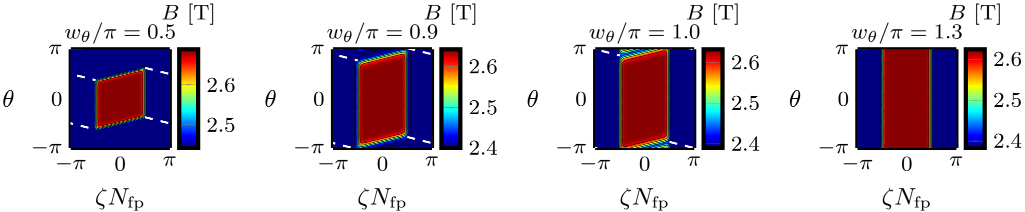

- Rough approximations to pwO can have low levels of radial transport. For $p = 2$ a banana-like regime appears.

3. Exploring pwO configuration space: from pwO to QI

Direct optimization of fast-ion confinement [Bindel, JPP (2023)] has inspired a new ideal design goal: piecewise omnigeneity (pwO) [Velasco, arXiv (2024)]. In a pwO magnetic field, $J = \oint v_\parallel \, \mathrm{d}l$ is a flux-function **piecewisely**. A simple pwO magnetic field is given by

$$B(\theta,\zeta) \sim B_{\min} + (B_{\max} - B_{\min}) \exp\left(- \left(\frac{\theta - t_\zeta \zeta}{w_\theta} \right)^{2p} - \left(\frac{\zeta}{w_\zeta} \right)^{2p} \right), \qquad \iota = -t_\zeta \frac{w_\zeta N_{\mathrm{fp}}}{\pi - w_\zeta N_{\mathrm{fp}}}$$

in the limit $p \to \infty$. For $w_\theta/\pi > 1$, the field becomes nearly QI. Example with $p = 10$.

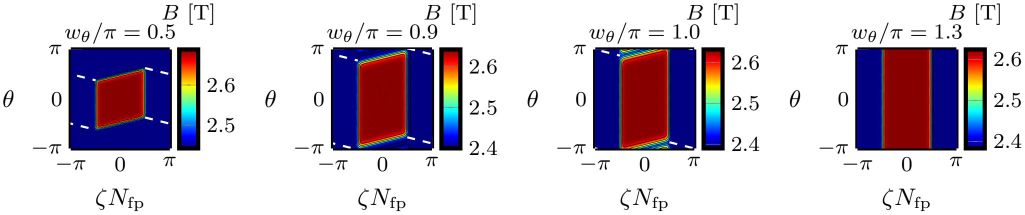

- Rough approximations to pwO can have low levels of radial transport. For $p = 2$ a banana-like regime appears.

In order to identify regions of pwO parameter space with small $\widehat{D}_{11}$ and $|\widehat{D}_{31}|$, a scan in w_θ and p has been carried out. Proximity to QI is controlled by w_θ and proximity to pwO by p.

3. Exploring pwO configuration space: from pwO to QI

The $\widehat{D}_{11}$ and $\widehat{D}_{31}$ coefficients have been evaluated using `MONKES`.

The $\widehat{D}_{11}$ and $\widehat{D}_{31}$ coefficients have been evaluated using `MONKES`.

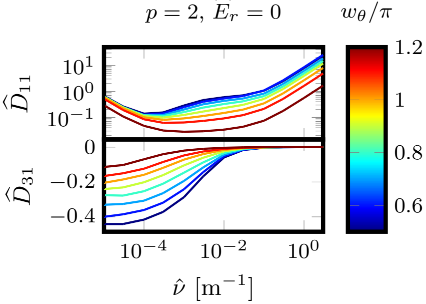

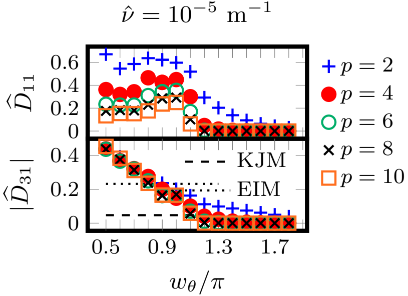

The $\widehat{D}_{11}$ and $\widehat{D}_{31}$ coefficients have been evaluated using `MONKES`.

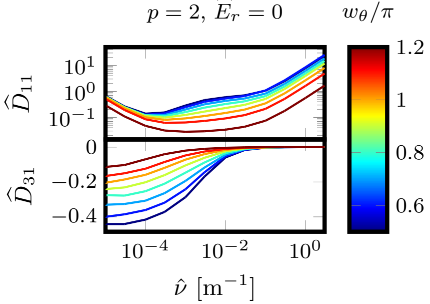

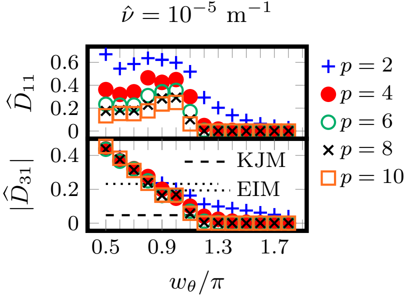

- As expected, $\widehat{D}_{11}$ is a decreasing function of p and $\widehat{D}_{31}$ a decreasing function of w_θ. For $p \geq 4$ and $w_\theta/\pi \geq 1.2$, smaller $|\widehat{D}_{31}|$ than W7X-KJM.

3. Exploring pwO configuration space: from pwO to QI

The $\widehat{D}_{11}$ and $\widehat{D}_{31}$ coefficients have been evaluated using `MONKES`.

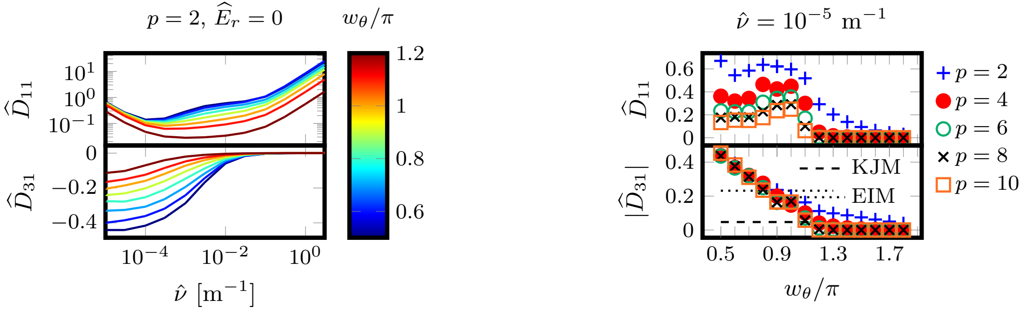

- As expected, $\widehat{D}_{11}$ is a decreasing function of p and $\widehat{D}_{31}$ a decreasing function of w_θ. For $p \geq 4$ and $w_\theta/\pi \geq 1.2$, smaller $|\widehat{D}_{31}|$ than W7X-KJM.
- Due to the large gradients of B, solving the DKE for this model magnetic field at $\hat{\nu} = 10^{-5}$ m^{-1} and $p = 10$ requires $N_{\text{fs}} \sim O(10^4)$ and $N_\xi \sim 200$. This could hardly be done with standard neoclassical codes.

3. Exploring pwO configuration space: from pwO to QI

The $\widehat{D}_{11}$ and $\widehat{D}_{31}$ coefficients have been evaluated using `MONKES`.

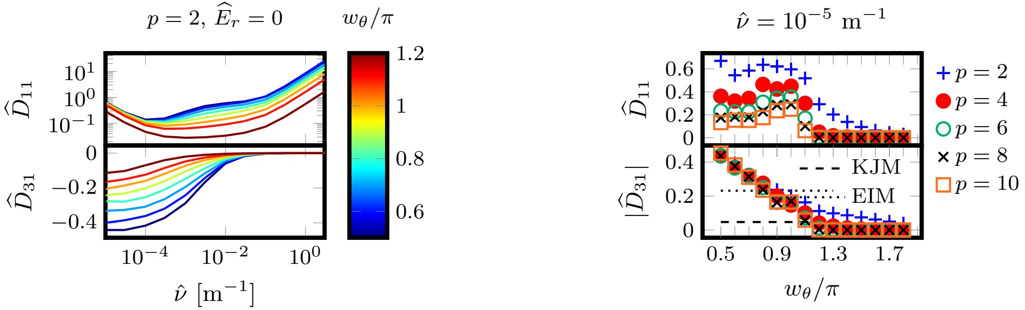

- As expected, $\widehat{D}_{11}$ is a decreasing function of p and $\widehat{D}_{31}$ a decreasing function of w_θ. For $p \geq 4$ and $w_\theta/\pi \geq 1.2$, smaller $|\widehat{D}_{31}|$ than W7X-KJM.
- Due to the large gradients of B, solving the DKE for this model magnetic field at $\hat{\nu} = 10^{-5}$ m^{-1} and $p = 10$ requires $N_{\text{fs}} \sim O(10^4)$ and $N_\xi \sim 200$. This could hardly be done with standard neoclassical codes.

`MONKES` can be used to explore extremely complicated magnetic fields. Magnetic fields can, in principle, deviate from QI to approach pwO while having low $\widehat{D}_{11}$ and $|\widehat{D}_{31}|$.

Outline

Conclusions and future work

- `MONKES` is a new neoclassical code which is much faster, flexible and accessible than `DKES`.
  - `MONKES` is sufficiently fast to be included in stellarator optimization suites.
  - `MONKES` can also provide derivatives of all the transport coefficients.

Conclusions and future work

- MONKES is a new neoclassical code which is much faster, flexible and accessible than DKES.
  - MONKES is sufficiently fast to be included in stellarator optimization suites.
  - MONKES can also provide derivatives of all the transport coefficients.

- MONKES transport coefficients can be used to compute neoclassical fluxes and flows associated to momentum-conserving collision operators [Maaßberg, PoP (2009)].

Conclusions and future work

- `MONKES` is a new neoclassical code which is much faster, flexible and accessible than `DKES`.
  - `MONKES` is sufficiently fast to be included in stellarator optimization suites.
  - `MONKES` can also provide derivatives of all the transport coefficients.

- `MONKES` transport coefficients can be used to compute neoclassical fluxes and flows associated to momentum-conserving collision operators [Maaßberg, PoP (2009)].

- `MONKES` is sufficiently fast to be included in predictive transport frameworks.

Conclusions and future work

- MONKES is a new neoclassical code which is much faster, flexible and accessible than DKES.
  - MONKES is sufficiently fast to be included in stellarator optimization suites.
  - MONKES can also provide derivatives of all the transport coefficients.

- MONKES transport coefficients can be used to compute neoclassical fluxes and flows associated to momentum-conserving collision operators [Maaßberg, PoP (2009)].

- MONKES is sufficiently fast to be included in predictive transport frameworks.
  - Although not as fast as KNOSOS for computing radial fluxes at low collisionality, permits to treat the transition from the $1/\nu$ or $\sqrt{\nu}$-ν to the plateau or banana regime transition.

Conclusions and future work

- MONKES is a new neoclassical code which is much faster, flexible and accessible than DKES.
  - MONKES is sufficiently fast to be included in stellarator optimization suites.
  - MONKES can also provide derivatives of all the transport coefficients.

- MONKES transport coefficients can be used to compute neoclassical fluxes and flows associated to momentum-conserving collision operators [Maaßberg, PoP (2009)].

- MONKES is sufficiently fast to be included in predictive transport frameworks.
  - Although not as fast as KNOSOS for computing radial fluxes at low collisionality, permits to treat the transition from the $1/\nu$ or $\sqrt{\nu}$-ν to the plateau or banana regime transition.
  - Opens up the possibility of introducing the bootstrap curent effect in **predictive transport simulations**.

EXTRA SLIDES

DKES convergence curves: W7-X EIM

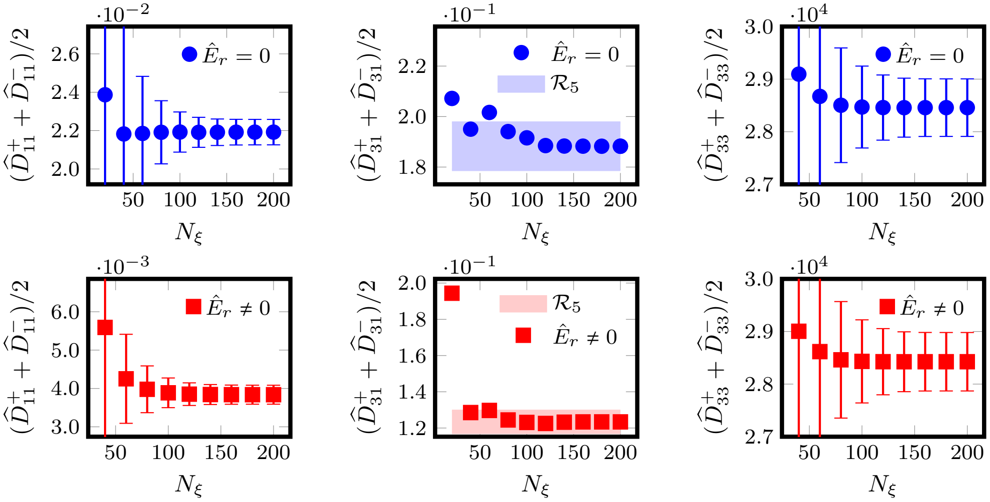

DKES convergence curves: W7-X KJM

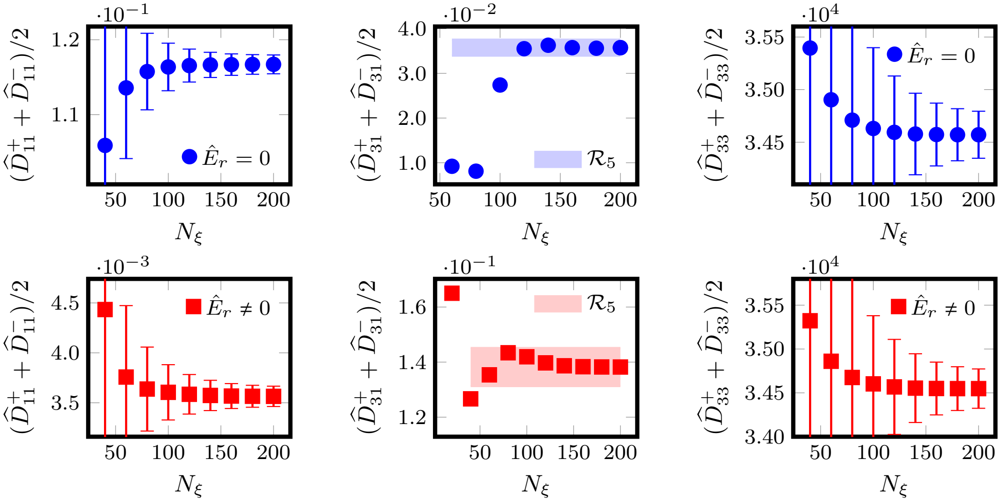

DKES convergence curves: CIEMAT-QI

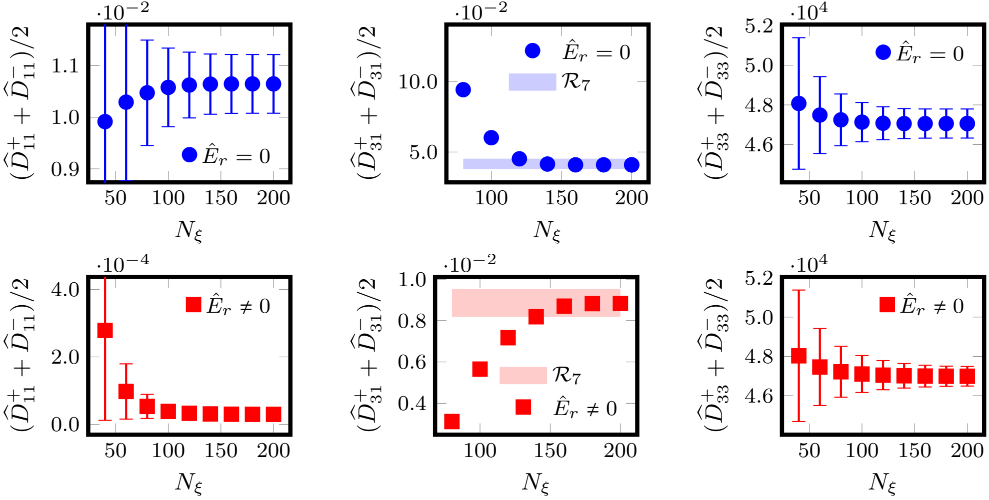

Thermal transport coefficients

Given the monoenergetic coefficients $\widehat{D}_{ij}$ as function of $\hat{\nu}(v)$ and fixed E_ψ ($\widehat{E}_\psi$ can vary), we can easily calculate the thermal coefficients

$$L_{ija}(\psi) = \frac{2n_a}{\sqrt{\pi}} \int_0^\infty x_a^2 e^{-x_a^2} w_i w_j K_{ija} \widehat{D}_{ij} \left(\psi, \hat{\nu}(x_a v_{\mathrm{t}a})\right) \mathrm{d}x_a \,,$$

where $x_a = v/v_{\mathrm{t}a}$ is the normalized speed.

Thermal transport coefficients

Given the monoenergetic coefficients $\widehat{D}_{ij}$ as function of $\hat{\nu}(v)$ and fixed E_ψ ($\widehat{E}_\psi$ can vary), we can easily calculate the thermal coefficients

$$L_{ija}(\psi) = \frac{2n_a}{\sqrt{\pi}} \int_0^\infty x_a^2 e^{-x_a^2} w_i w_j K_{ija} \widehat{D}_{ij}\left(\psi, \hat{\nu}(x_a v_{\mathrm{t}a})\right) \mathrm{d}x_a \, ,$$

where $x_a = v/v_{\mathrm{t}a}$ is the normalized speed.

- `MONKES` uses Gaussian quadratures based on Maxwell polynomials [Landreman and Ernst, JCP (2012)] for computing the integrals in x_a. Convergence for $N_{x_a} \sim 10 - 20$.

Thermal transport coefficients

Given the monoenergetic coefficients $\widehat{D}_{ij}$ as function of $\hat{\nu}(v)$ and fixed E_ψ ($\widehat{E}_\psi$ can vary), we can easily calculate the thermal coefficients

$$L_{ija}(\psi) = \frac{2n_a}{\sqrt{\pi}} \int_0^\infty x_a^2 e^{-x_a^2} w_i w_j K_{ija} \widehat{D}_{ij} \left(\psi, \hat{\nu}(x_a v_{\mathrm{t}a})\right) \mathrm{d}x_a \,,$$

where $x_a = v/v_{\mathrm{t}a}$ is the normalized speed.

- `MONKES` uses Gaussian quadratures based on Maxwell polynomials [Landreman and Ernst, JCP (2012)] for computing the integrals in x_a. Convergence for $N_{x_a} \sim 10 - 20$.
- Each calculation of $\widehat{D}_{ij}$ can be computed in parallel $\Rightarrow$ Fast calculation of neoclassical fluxes in the Lorentz limit.

Thermal transport coefficients

Given the monoenergetic coefficients $\widehat{D}_{ij}$ as function of $\hat{\nu}(v)$ and fixed E_ψ ($\widehat{E}_\psi$ can vary), we can easily calculate the thermal coefficients

$$L_{ija}(\psi) = \frac{2n_a}{\sqrt{\pi}} \int_0^\infty x_a^2 e^{-x_a^2} w_i w_j K_{ija} \widehat{D}_{ij}\left(\psi, \hat{\nu}(x_a v_{ta})\right) \mathrm{d}x_a \, ,$$

where $x_a = v/v_{ta}$ is the normalized speed.

- `MONKES` uses Gaussian quadratures based on Maxwell polynomials [Landreman and Ernst, JCP (2012)] for computing the integrals in x_a. Convergence for $N_{x_a} \sim 10-20$.
- Each calculation of $\widehat{D}_{ij}$ can be computed in parallel $\Rightarrow$ Fast calculation of neoclassical fluxes in the Lorentz limit.
- Fluxes in the Lorentz limit can be used to calculate neoclassical fluxes for more refined momentum-conserving collision operators [Maaßberg, PoP (2009)] with negligible extra computational cost.

Thermal transport coefficients

Given the monoenergetic coefficients $\widehat{D}_{ij}$ as function of $\hat{\nu}(v)$ and fixed E_ψ ($\widehat{E}_\psi$ can vary), we can easily calculate the thermal coefficients

$$L_{ija}(\psi) = \frac{2n_a}{\sqrt{\pi}} \int_0^\infty x_a^2 e^{-x_a^2} w_i w_j K_{ija} \widehat{D}_{ij}\left(\psi, \hat{\nu}(x_a v_{ta})\right) \mathrm{d}x_a \,,$$

where $x_a = v/v_{ta}$ is the normalized speed.

- `MONKES` uses Gaussian quadratures based on Maxwell polynomials [Landreman and Ernst, JCP (2012)] for computing the integrals in x_a. Convergence for $N_{x_a} \sim 10 - 20$.
- Each calculation of $\widehat{D}_{ij}$ can be computed in parallel $\Rightarrow$ Fast calculation of neoclassical fluxes in the Lorentz limit.
- Fluxes in the Lorentz limit can be used to calculate neoclassical fluxes for more refined momentum-conserving collision operators [Maaßberg, PoP (2009)] with negligible extra computational cost.

`MONKES` will (soon) provide quick calculations of radial fluxes and parallel flows in multispecies stellarator plasmas.

Benchmark of neoclassical fluxes

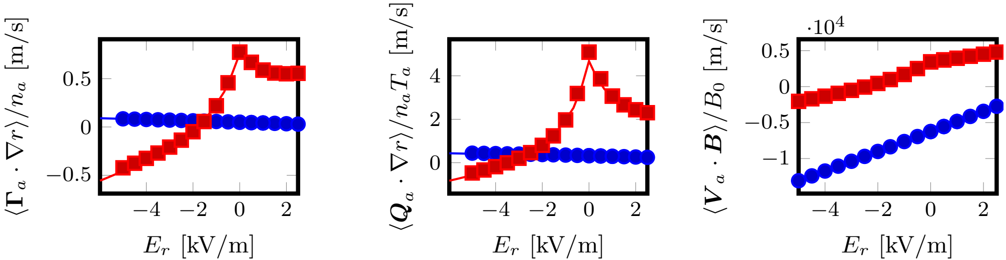

Direct approach for computing derivatives of the transport coefficients

Suppose $\eta \in \{\hat{\nu}, \widehat{E}_\psi, \{B_{mn}\}_{mn\in\mathbb{Z}}, \iota, B_\zeta, B_\theta, \ldots\}$ is a parameter upon which the DKE depends. For gradient-based optimization methods (among other things) it is useful to compute

$$\frac{\partial \widehat{D}_{ij}}{\partial \eta} = \left\langle \frac{1}{\sqrt{g}} \int_{-1}^{1} \sqrt{g} s_i \frac{\partial f_j}{\partial \eta} \, \mathrm{d}\xi \right\rangle + \left\langle \frac{1}{\sqrt{g}} \int_{-1}^{1} \frac{\partial(\sqrt{g} s_i)}{\partial \eta} f_j \, \mathrm{d}\xi \right\rangle.$$

Direct approach for computing derivatives of the transport coefficients

Suppose $\eta \in \{\hat{\nu}, \widehat{E}_\psi, \{B_{mn}\}_{mn\in\mathbb{Z}}, \iota, B_\zeta, B_\theta, \dots\}$ is a parameter upon which the DKE depends. For gradient-based optimization methods (among other things) it is useful to compute

$$\frac{\partial \widehat{D}_{ij}}{\partial \eta} = \left\langle \frac{1}{\sqrt{g}} \int_{-1}^{1} \sqrt{g} s_i \frac{\partial f_j}{\partial \eta} \,\mathrm{d}\xi \right\rangle + \left\langle \frac{1}{\sqrt{g}} \int_{-1}^{1} \frac{\partial(\sqrt{g} s_i)}{\partial \eta} f_j \,\mathrm{d}\xi \right\rangle.$$

We can obtain the equation for $\partial f_j/\partial\eta$ deriving the DKE along η

$$L_k \frac{\partial f^{(k-1)}}{\partial \eta} + D_k \frac{\partial f^{(k)}}{\partial \eta} + U_k \frac{\partial f^{(k+1)}}{\partial \eta} = \frac{\partial s^{(k)}}{\partial \eta} - L_{k,\eta} f^{(k-1)} - D_{k,\eta} f^{(k)} - U_{k,\eta} f^{(k+1)},$$

where $L_{k,\eta}$, $D_{k,\eta}$ and $U_{k,\eta}$ are operators whose coefficients are the derivatives of those of L_k, D_k and U_k.

Direct approach for computing derivatives of the transport coefficients

Suppose $\eta \in \{\hat{\nu}, \widehat{E}_\psi, \{B_{mn}\}_{mn\in\mathbb{Z}}, \iota, B_\zeta, B_\theta, \ldots\}$ is a parameter upon which the DKE depends. For gradient-based optimization methods (among other things) it is useful to compute

$$\frac{\partial \widehat{D}_{ij}}{\partial \eta} = \left\langle \frac{1}{\sqrt{g}} \int_{-1}^{1} \sqrt{g} s_i \frac{\partial f_j}{\partial \eta} \, \mathrm{d}\xi \right\rangle + \left\langle \frac{1}{\sqrt{g}} \int_{-1}^{1} \frac{\partial(\sqrt{g} s_i)}{\partial \eta} f_j \, \mathrm{d}\xi \right\rangle.$$

We can obtain the equation for $\partial f_j / \partial \eta$ deriving the DKE along η

$$L_k \frac{\partial f^{(k-1)}}{\partial \eta} + D_k \frac{\partial f^{(k)}}{\partial \eta} + U_k \frac{\partial f^{(k+1)}}{\partial \eta} = \frac{\partial s^{(k)}}{\partial \eta} - L_{k,\eta} f^{(k-1)} - D_{k,\eta} f^{(k)} - U_{k,\eta} f^{(k+1)},$$

where $L_{k,\eta}$, $D_{k,\eta}$ and $U_{k,\eta}$ are operators whose coefficients are the derivatives of those of L_k, D_k and U_k. This equation has been solved for a different source term!

Direct approach for computing derivatives of the transport coefficients

Suppose $\eta \in \{\hat{\nu}, \widehat{E}_\psi, \{B_{mn}\}_{mn\in\mathbb{Z}}, \iota, B_\zeta, B_\theta, \ldots\}$ is a parameter upon which the DKE depends. For gradient-based optimization methods (among other things) it is useful to compute

$$\frac{\partial \widehat{D}_{ij}}{\partial \eta} = \left\langle \frac{1}{\sqrt{g}} \int_{-1}^{1} \sqrt{g} s_i \frac{\partial f_j}{\partial \eta}\, \mathrm{d}\xi \right\rangle + \left\langle \frac{1}{\sqrt{g}} \int_{-1}^{1} \frac{\partial(\sqrt{g} s_i)}{\partial \eta} f_j\, \mathrm{d}\xi \right\rangle.$$

We can obtain the equation for $\partial f_j/\partial\eta$ deriving the DKE along η

$$L_k \frac{\partial f^{(k-1)}}{\partial \eta} + D_k \frac{\partial f^{(k)}}{\partial \eta} + U_k \frac{\partial f^{(k+1)}}{\partial \eta} = \frac{\partial s^{(k)}}{\partial \eta} - L_{k,\eta} f^{(k-1)} - D_{k,\eta} f^{(k)} - U_{k,\eta} f^{(k+1)},$$

where $L_{k,\eta}$, $D_{k,\eta}$ and $U_{k,\eta}$ are operators whose coefficients are the derivatives of those of L_k, D_k and U_k. This equation has been solved for a different source term!

- For calculating $\partial\widehat{D}_{ij}/\partial\eta$ we only need to solve for $\{\partial f^{(k)}/\partial\eta\}_{k=0}^{2}$.

Direct approach for computing derivatives of the transport coefficients

Suppose $\eta \in \{\hat{\nu}, \widehat{E}_\psi, \{B_{mn}\}_{mn\in\mathbb{Z}}, \iota, B_\zeta, B_\theta, \ldots\}$ is a parameter upon which the DKE depends. For gradient-based optimization methods (among other things) it is useful to compute

$$\frac{\partial \widehat{D}_{ij}}{\partial \eta} = \left\langle \frac{1}{\sqrt{g}} \int_{-1}^{1} \sqrt{g} s_i \frac{\partial f_j}{\partial \eta}\, \mathrm{d}\xi \right\rangle + \left\langle \frac{1}{\sqrt{g}} \int_{-1}^{1} \frac{\partial(\sqrt{g} s_i)}{\partial \eta} f_j \,\mathrm{d}\xi \right\rangle.$$

We can obtain the equation for $\partial f_j/\partial\eta$ deriving the DKE along η

$$L_k \frac{\partial f^{(k-1)}}{\partial \eta} + D_k \frac{\partial f^{(k)}}{\partial \eta} + U_k \frac{\partial f^{(k+1)}}{\partial \eta} = \frac{\partial s^{(k)}}{\partial \eta} - L_{k,\eta} f^{(k-1)} - D_{k,\eta} f^{(k)} - U_{k,\eta} f^{(k+1)},$$

where $L_{k,\eta}$, $D_{k,\eta}$ and $U_{k,\eta}$ are operators whose coefficients are the derivatives of those of L_k, D_k and U_k. This equation has been solved for a different source term!

- For calculating $\partial\widehat{D}_{ij}/\partial\eta$ we only need to solve for $\{\partial f^{(k)}/\partial\eta\}_{k=0}^{2}$.
- By reusing the LU factorizations from forward elimination, we can solve for N_η derivatives of $\widehat{D}_{ij}$ in $O(N_\eta N_{\mathrm{fs}}^2)$ operations once $\{f^{(k)}\}_{k=0}^{N_\xi}$ is known ($O(N_\xi N_{\mathrm{fs}}^3)$ operations).

Direct approach for computing derivatives of the transport coefficients

Suppose $\eta \in \{\hat{\nu}, \widehat{E}_\psi, \{B_{mn}\}_{mn\in\mathbb{Z}}, \iota, B_\zeta, B_\theta, \ldots\}$ is a parameter upon which the DKE depends. For gradient-based optimization methods (among other things) it is useful to compute

$$\frac{\partial \widehat{D}_{ij}}{\partial \eta} = \left\langle \frac{1}{\sqrt{g}} \int_{-1}^{1} \sqrt{g} s_i \frac{\partial f_j}{\partial \eta} \, \mathrm{d}\xi \right\rangle + \left\langle \frac{1}{\sqrt{g}} \int_{-1}^{1} \frac{\partial(\sqrt{g} s_i)}{\partial \eta} f_j \, \mathrm{d}\xi \right\rangle.$$

We can obtain the equation for $\partial f_j / \partial \eta$ deriving the DKE along η

$$L_k \frac{\partial f^{(k-1)}}{\partial \eta} + D_k \frac{\partial f^{(k)}}{\partial \eta} + U_k \frac{\partial f^{(k+1)}}{\partial \eta} = \frac{\partial s^{(k)}}{\partial \eta} - L_{k,\eta} f^{(k-1)} - D_{k,\eta} f^{(k)} - U_{k,\eta} f^{(k+1)},$$

where $L_{k,\eta}$, $D_{k,\eta}$ and $U_{k,\eta}$ are operators whose coefficients are the derivatives of those of L_k, D_k and U_k. This equation has been solved for a different source term!

- For calculating $\partial \widehat{D}_{ij} / \partial \eta$ we only need to solve for $\{\partial f^{(k)} / \partial \eta\}_{k=0}^{2}$.
- By reusing the LU factorizations from forward elimination, we can solve for N_η derivatives of $\widehat{D}_{ij}$ in $O(N_\eta N_{\mathrm{fs}}^2)$ operations once $\{f^{(k)}\}_{k=0}^{N_\xi}$ is known ($O(N_\xi N_{\mathrm{fs}}^3)$ operations).
- For $N_\eta \lesssim N_\xi N_{\mathrm{fs}}$ the direct method is faster than an adjoint method.

Contribution of different classes of particles to $\widehat{D}_{ij}$

Contribution to the monoenergetic coefficient $\widehat{D}_{ij}$ of particles with $\lambda' \in [0, \lambda]$ where $\lambda := v_\perp^2/Bv^2 = (1-\xi^2)/B \in [0, B_{\min}^{-1}]$

$$\widehat{d}_{ij}(\lambda) := \widehat{D}_{ij} - \left\langle \int_{-1}^{1} s_i f_j H(1 - \lambda B - \xi^2)\, \mathrm{d}\xi \right\rangle.$$

- For $\lambda < \lambda_\mathrm{c} = 1/B_{\max}$, $|\xi|(\lambda, B) = \sqrt{1 - \lambda B} > 0$. **Passing**.
- For $\lambda > \lambda_\mathrm{c}$, $|\xi|(\lambda, B) = \sqrt{1 - \lambda B} = 0$ if $\lambda B = 1$. **Trapped**.

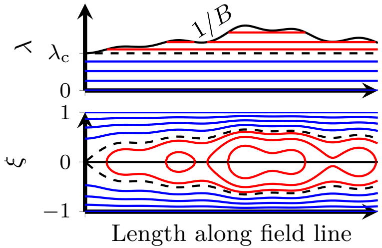

Contribution of different classes of particles to $\widehat{D}_{ij}$

Contribution to the monoenergetic coefficient $\widehat{D}_{ij}$ of particles with $\lambda' \in [0, \lambda]$ where $\lambda := v_\perp^2/Bv^2 = (1-\xi^2)/B \in [0, B_{\mathrm{min}}^{-1}]$

$$\widehat{d}_{ij}(\lambda) := \widehat{D}_{ij} - \left\langle \int_{-1}^{1} s_i f_j H(1 - \lambda B - \xi^2)\, \mathrm{d}\xi \right\rangle.$$

- For $\lambda < \lambda_{\mathrm{c}} = 1/B_{\mathrm{max}}$, $|\xi|(\lambda, B) = \sqrt{1-\lambda B} > 0$. **Passing**.
- For $\lambda > \lambda_{\mathrm{c}}$, $|\xi|(\lambda, B) = \sqrt{1-\lambda B} = 0$ if $\lambda B = 1$. **Trapped**.

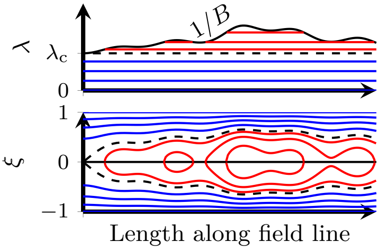

MONKES allows to verify analytical results [Boozer, Phys. Fluids (1990)], [Calvo, PPCF (2017)]

Contribution of different classes of particles to $\widehat{D}_{ij}$

Contribution to the monoenergetic coefficient $\widehat{D}_{ij}$ of particles with $\lambda' \in [0, \lambda]$ where $\lambda := v_\perp^2/Bv^2 = (1-\xi^2)/B \in [0, B_{\min}^{-1}]$

$$\widehat{d}_{ij}(\lambda) := \widehat{D}_{ij} - \left\langle \int_{-1}^{1} s_i f_j H(1 - \lambda B - \xi^2)\,\mathrm{d}\xi \right\rangle.$$

- For $\lambda < \lambda_\mathrm{c} = 1/B_{\max}$, $|\xi|(\lambda, B) = \sqrt{1-\lambda B} > 0$. **Passing**.
- For $\lambda > \lambda_\mathrm{c}$, $|\xi|(\lambda, B) = \sqrt{1-\lambda B} = 0$ if $\lambda B = 1$. **Trapped**.

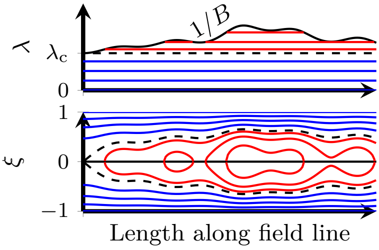

MONKES allows to verify analytical results [Boozer, Phys. Fluids (1990)], [Calvo, PPCF (2017)]

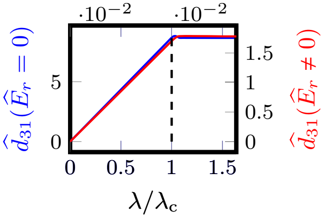

CIEMAT-QI

Contribution of different classes of particles to $\widehat{D}_{ij}$

Contribution to the monoenergetic coefficient $\widehat{D}_{ij}$ of particles with $\lambda' \in [0,\lambda]$ where $\lambda := v_\perp^2/Bv^2 = (1-\xi^2)/B \in [0, B_{\min}^{-1}]$

$$\widehat{d}_{ij}(\lambda) := \widehat{D}_{ij} - \left\langle \int_{-1}^{1} s_i f_j H(1-\lambda B - \xi^2)\,\mathrm{d}\xi \right\rangle.$$

- For $\lambda < \lambda_c = 1/B_{\max}$, $|\xi|(\lambda, B) = \sqrt{1-\lambda B} > 0$. **Passing**.
- For $\lambda > \lambda_c$, $|\xi|(\lambda, B) = \sqrt{1-\lambda B} = 0$ if $\lambda B = 1$. **Trapped**.

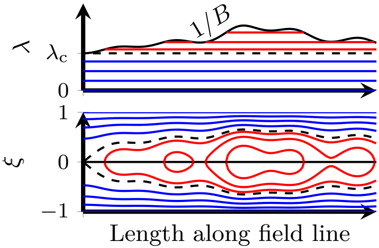

MONKES allows to verify analytical results [Boozer, Phys. Fluids (1990)], [Calvo, PPCF (2017)]

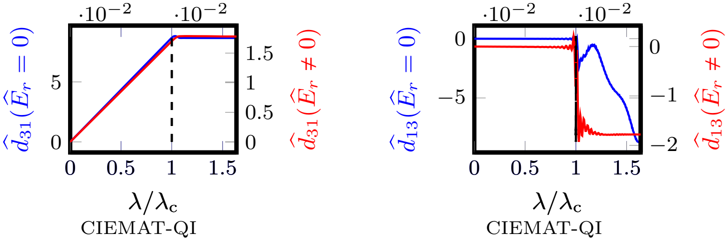

Contribution of different classes of particles to $\widehat{D}_{ij}$

Contribution to the monoenergetic coefficient $\widehat{D}_{ij}$ of particles with $\lambda' \in [0, \lambda]$ where $\lambda := v_\perp^2/Bv^2 = (1-\xi^2)/B \in [0, B_{\text{min}}^{-1}]$

$$\widehat{d}_{ij}(\lambda) := \widehat{D}_{ij} - \left\langle \int_{-1}^{1} s_i f_j H(1-\lambda B - \xi^2)\,\mathrm{d}\xi \right\rangle.$$

- For $\lambda < \lambda_\mathrm{c} = 1/B_\mathrm{max}$, $|\xi|(\lambda, B) = \sqrt{1-\lambda B} > 0$. **Passing**.
- For $\lambda > \lambda_\mathrm{c}$, $|\xi|(\lambda, B) = \sqrt{1-\lambda B} = 0$ if $\lambda B = 1$. **Trapped**.

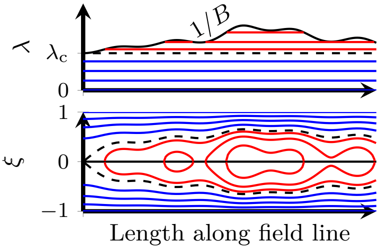

MONKES allows to verify analytical results [Boozer, Phys. Fluids (1990)], [Calvo, PPCF (2017)]

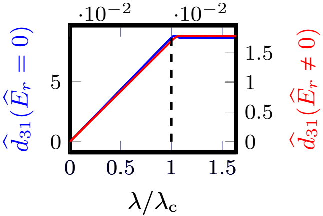

CIEMAT-QI

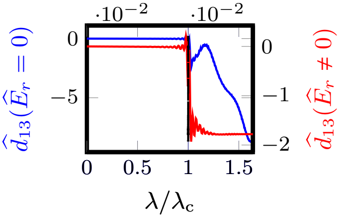

CIEMAT-QI

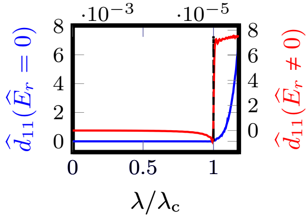

QH Landreman & Paul